Switching on H-tunneling through conformational control

SCHOLARONE™
Manuscripts

Switching on H-tunneling through conformational control

José P. L. Roque,[1] Cláudio M. Nunes,[1]* Luís P. Viegas,[1] Nelson A. M. Pereira,[1] Teresa M. V. D. Pinho e Melo,[1] Peter R. Schreiner,[2] and Rui Fausto[1]

[1]University of Coimbra, CQC, Department of Chemistry, 3004-535 Coimbra, Portugal

[2]Institute of Organic Chemistry, Justus Liebig University, Heinrich-Buff-Ring 17, 35392 Giessen, Germany
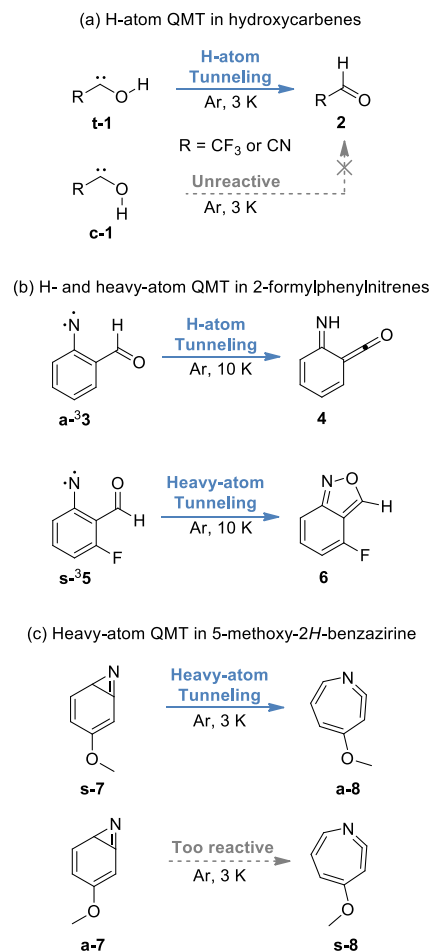
Supporting Information Placeholder

ABSTRACT: H-tunneling is a ubiquitous phenomenon, relevant to fields from biochemistry to materials science, but harnessing it for mastering the manipulation of chemical structures still remains nearly illusory. Here, we demonstrate how to switch on H-tunneling by conformational control using external radiation. This is outlined with a triplet 2-hydroxyphenylnitrene generated in an N_2 matrix at 10 K by UV-irradiation of an azide precursor. The *anti*-orientation of its OH moiety was converted to *syn* by selective vibrational excitation at the $2\nu(OH)$ frequency, thereby moving the H-atom closer to the vicinal nitrene center. This triggers spontaneous H-tunneling to a singlet 6-imino-2,4-cyclohexadienone. Computations unravel that such fast H-tunneling occurs through crossing the triplet-to-singlet potential energy surfaces. Our experimental realization provides an exciting novel strategy to attain control over tunneling, opening new avenues for directing chemical transformations.

Molecular conformers can dictate the reactivity of chemical[1,2] and biological systems,[3,4] materials functions,[5,6] and even control anticancer activity.[7] However, it is still challenging to understand how different conformers can lead to different reactions paths or kinetics and what conditions allow conformational control of reactants.[8–10] Conformational changes are difficult to assess at ambient conditions due to their typically observed fast interconversions. Nonetheless, a few conformer-specific reactions have been demonstrated under low-temperature conditions, paving the way for a better understanding of the conformational influence on the selectivity of chemical reactions and functions.[11–16]

Quantum mechanical tunneling (QMT) is very sensitive to the distances nuclei move in a reaction,[17–20] therefore the conformation of a reactive moiety can become critical for the occurrence of QMT.[21] Indeed, one of us recently demonstrated the first examples of conformer dependent H-atom QMT (Scheme 1a).[22,23] After trapping hydroxycarbenes **1** in argon matrices at temperatures as low as 3 K, we observed that the *trans*-conformer **t-1** rearranges by QMT to aldehyde **2**, whereas the *cis*-conformer **c-1** remained unreactive. We have also demonstrated that different conformations of an aldehyde moiety in the vicinity of a nitrene center give access to different QMT reactions (Scheme 1b).[24,25] It was observed that the *anti*-conformer **a-³3**, once generated in argon matrices, rearranges by H-atom QMT to imino-ketene **4** whereas the *syn*-conformer **s-³5** cyclizes by heavy-atom QMT to 2,1-benzisoxazole **6**. Moreover, a rare example of conformer dependent heavy-atom QMT was reported by Sander *et al.*[26,27] They observed by matrix isolation spectroscopy that *syn*-5-methoxy-

2*H*-benzazirine **s-7** rearranges by QMT to ketenimine **a-8**, while the *anti*-conformer **a-7** is too reactive to be detected (Scheme 1c). It has been also suggested that enzymatic C–H transfer reactions rely on the dynamic sampling of enzyme-substrate conformations to tune the donor-acceptor distance conductive to QMT.[28,29] Structural enzymatic modifications either near the bound substrate or at a remote residue has been argued to influence H-atom QMT through changes in conformational flexibility.[30–33]

Scheme 1. Examples of conformer-dependent QMT reactions directly observed by matrix isolation spectroscopy[34]

(a) H-atom QMT in hydroxycarbenes

(b) H- and heavy-atom QMT in 2-formylphenylnitrenes

(c) Heavy-atom QMT in 5-methoxy-2*H*-benzazirine

While these investigations have begun to decipher how QMT reactivity can significantly depend on conformations, even in moieties remotely located in relation to the reaction center, further breakthroughs can be envisaged through effective conformational control of reactants. Thus, we demonstrate here the experimental realization of how to switch on a QMT reaction through selective conversion of an unreactive to a reactive conformer using vibrational excitation (Scheme 2).[35] Controlled manipulation of *anti*-OH triplet 3-fluoro-2-hydroxyphenylnitrene **a-³10** to the reactive *syn*-OH conformer **s-³10** was achieved in an N₂ matrix at 10 K by narrowband irradiation at the 2ν(OH) frequency, triggering fast H-atom QMT to singlet 2-fluoro-6-imino-2,4-cyclohexadienone **Z-11**. Computations unravel that such fast H-atom QMT occurs through crossing potential energy surfaces (PESs).

Scheme 2. Summary of the H-atom QMT of 2-hydroxyphenylnitrene s-³10 to imino Z-11 switched on upon conformational isomerization of a-³10 by vibrational excitation
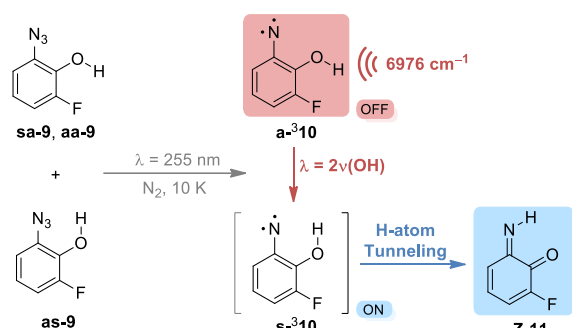
The photolysis of parent 2-hydroxyphenylazide **9'** under matrix isolation conditions was independently studied by Sander *et al.*[36] and Tomioka *et al.*[37] Both groups reported the formation of an *E/Z* mixture of 6-imino-2,4-cyclohexadienone **11'**, presumably via [1,4]-H shift reaction of 2-hydroxyphenylnitrene **10'**. However, neither group detected ground-state triplet nitrene **³10'** by matrix isolation spectroscopy. Considering the short distance [2.28 Å at B3LYP/6-311+G(2d,p)] between the nitrene center and the hydrogen atom of the OH moiety in *syn*-conformation, it is likely that the [1,4]-H shift occurs by fast H-atom QMT, making **s-³10'** elusive.[38] On the other hand, the longer distance [3.73 Å at B3LYP/6-311+G(2d,p)] between the nitrene center and the hydrogen atom of the OH moiety in the *anti*-conformation makes H-atom QMT unlikely and the capture of **a-³10'** conceivable under cryogenic temperatures. The lack of detection of **a-³10'** could be due to the preservation of the *syn*-OH conformation in the photolysis of **9'**,[39] as previously observed for the aldehyde conformation in the photolysis of 2-formylphenylazides (Scheme 1b).[24,25] CBS-QB3 computations indicate that **9'** in gas-phase at room temperature (r.t.) exclusively in the most stable conformation **as-9'**, with the OH moiety in *syn*-conformation relative to the N₃ moiety (Table S1).

To significantly populate the *anti*-OH conformer of 2-hydroxyphenylazides, we considered the inclusion of a vicinal fluorine atom acting as hydrogen-bond acceptor for the OH moiety, following the approach used to stabilize the more energetic aldehyde conformer in 2-formylphenylazides.[24] CBS-QB3 computations for the 3-fluoro-2-hydroxyphenylazide **9** predict the *anti*-OH conformers (**sa-9** and **aa-9**) to be only 2–4 kJ mol⁻¹ higher in energy than the most stable *syn*-OH conformer (**as-9**), i.e., a stabilization of ~10 kJ mol⁻¹ relatively to **9'** (Table S1).

Accordingly, the predicted gas-phase equilibrium population at r.t. consists of ~34% of the *anti*-OH and ~66% of the *syn*-OH conformers, indicating that **9** would be a promising system to access a 2-hydroxyphenylnitrene having an *anti*-OH conformation (**a-³10**).

3-Fluoro-2-hydroxyphenylazide **9** was synthesized and characterized as described in the SI. Matrices with monomers of **9** were prepared by sublimating the sample at r.t. and depositing it with a large excess of N₂ gas onto a CsI optical window (10 K). The IR spectrum of matrix-isolated **9** confirms the presence of both *syn*-OH and *anti*-OH conformers in a ratio that roughly mimics the predicted 66:34 ratio (Figures 1 and S1). This is particularly evident in the mid- and near-IR regions corresponding to the ν(OH) and 2ν(OH) modes (Figure 1). The lower frequency bands centered at 3557 and 6938 cm⁻¹ are assigned to the vibrational modes of *syn*-OH conformer **as-9** computed at 3573 [ν(OH)] and 6969 cm⁻¹ [2ν(OH)]. The slightly overlapping higher frequency bands centered at 3603 and 7039 cm⁻¹ as well as at ~3591 and ~7009 cm⁻¹ are assigned to the vibrational modes of the *anti*-OH conformers, **sa-9** and **aa-9**, computed at 3621 [ν(OH)] and 7074 cm⁻¹ [2ν(OH)], and at 3608 [ν(OH)] and 7045 cm⁻¹ [2ν(OH)], respectively.[40]
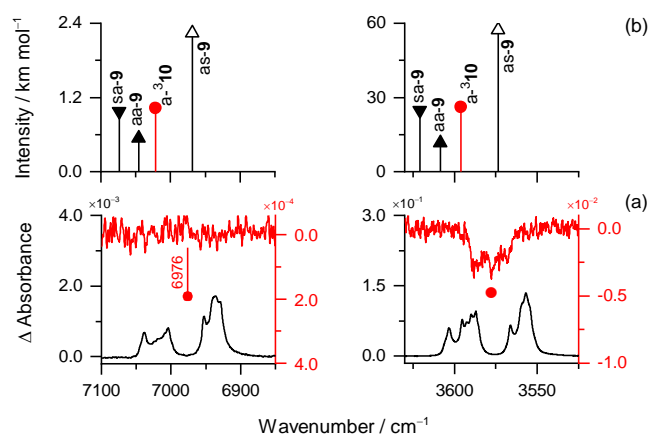

Figure 1. (a) Selected regions of the experimental mid-IR (right) and near-IR (left) spectrum collected immediately after the deposition of 3-fluoro-2-hydroxyphenylazide **9** in an N₂ matrix at 10 K (back line) and the corresponding difference IR spectrum (red line) resulting from irradiation at λ = 310 nm (10 min, 10 mW), subsequent to the full consumption of **9** with a set of irradiations at λ = 255 nm. The 2ν(OH) band of **a-³10** is inferred to be centered at ~6976 cm⁻¹. (b) B3LYP/6-311+G(2d,p) computed anharmonic wavenumbers and IR intensities for the ν(OH) (right) and 2ν(OH) (left) modes of **as-9**, **aa-9** and **sa-9** conformers (black triangles), and of **a-³10** (red circles). The intensities of **as-9**, **aa-9** and **sa-9** were scaled considering the computed population ratio of 66:11:23, respectively. The intensity of **a-³10** was scaled by an arbitrary factor.

The photolysis of **9** was then promoted by irradiations at λ = 255 or 280 nm [UV-Vis of **9** in acetonitrile: λmax = ~250 and 280 nm (Figure S3)] and found to lead to (*Z*)-2-fluoro-6-imino-2,4-cyclohexadienone **Z-11**, as the major product, and to the *anti*-OH conformer of 3-fluoro-2-hydroxyphenylnitrene **a-³10**, as the minor product (Figure S4). The most distinctive IR bands of **Z-11** appear as a broad feature at ~3216 cm⁻¹ and as two strong signals at 1691 and 1648 cm⁻¹, corresponding to the ν(NH), ν(C=O), and ν(C=C)as modes, whereas those of **a-³10** appear at ~3576 and 1571 cm⁻¹, corresponding to the ν(OH) and ν(CC) modes. The detailed assignment of the IR spectra of both products is addressed in the next section. The successful generation of nitrene

2

a-³10 in a nitrogen matrix at 10 K confirms our working hypothesis regarding the existence of an "unreactive" *anti*-OH conformer (a-³10) besides of a "reactive" *syn*-OH conformer (s-³10).[41]

It has been shown that energy can be selectively deposited in a vibrational mode of a molecular system and be transferred to a torsional reaction coordinate, via an intramolecular relaxation mechanism, for promoting conformational changes.[42–46] Efficient energy transfer to the torsional reaction coordinate is usually achieved if the stretching bond of the conformational moiety is excited to its first overtone.[46–49] To implement this approach and attain controlled switch of the "unreactive" a-³10 to the "reactive" s-³10, the 2ν(OH) frequency of a-³10 was examined. A dedicated experiment where 9 was totally consumed (λ = 255 nm) and then the remaining a-³10 was converted to 11 (λ = 310 nm), allowed the measurement of the ν(OH) band of a-³10 centered at ~3576 cm⁻¹, between the consumed ν(OH) bands of as-9 and aa-9 (Figure 1a). Unfortunately, the corresponding 2ν(OH) band was not detected, due to its broad and low absorption features alongside with the very small amount of a-³10 present in the matrix. Nevertheless, we can infer that the 2ν(OH) band of a-³10 should be centered at ~6976 cm⁻¹, between the 2ν(OH) bands of as-9 (~6938 cm⁻¹) and aa-9 (~7009 cm⁻¹), mirroring the pattern observed for the corresponding ν(OH) bands (Figure 1a). This rationalization is supported by B3LYP/6-311+G(2d,p) anharmonic computations, which estimated the ν(OH) and 2ν(OH) modes of a-³10 at frequencies between those of as-9 and aa-9 (Figure 1b).

The effect of selective vibrational excitation of a-³10 at its 2ν(OH) frequency was then explored. The irradiation of freshly generated a-³10 in an N₂ matrix at 10 K with narrowband light tuned to 6976 cm⁻¹ induces its transformation to Z-11.[50,51] The process was monitored by mid-IR spectroscopy using a long-pass filter blocking IR light above 1580 cm⁻¹ to exclude the absorption of photons above the OH-rotamerization barrier [a-³10 → s-³10; ~1700 cm⁻¹ at B3LYP/6-311+G(2d,p)]. The negative and positive bands of the experimental difference spectrum are well reproduced by the B3LYP/6-311+G(2d,p) computed spectra of a-³10 and Z-11, respectively (Figure 2). Some distinctive depleted bands are observed at 1538, 1444, 1303, 768/765, and 696 cm⁻¹, matching the characteristic vibration modes of a-³10 computed at 1536 [ν(CC)], 1433 [δ(CH)], 1298 [ν(CN)], 754 [γ(CH)], and 686 [ν(CC)] cm⁻¹. Representative produced bands are observed at 1256, 1164, 1114, 836, and 727 cm⁻¹, matching the characteristic vibration modes of Z-11 computed at 1241 [ν(CF)], 1163 [δ(CH)], 1098 [ν(C-C)], 828 [δ(ring)], and 723 [γ(CH)] cm⁻¹. A detailed assignment of the IR spectra of a-³10 and Z-11 is given in Tables S4 and S5.
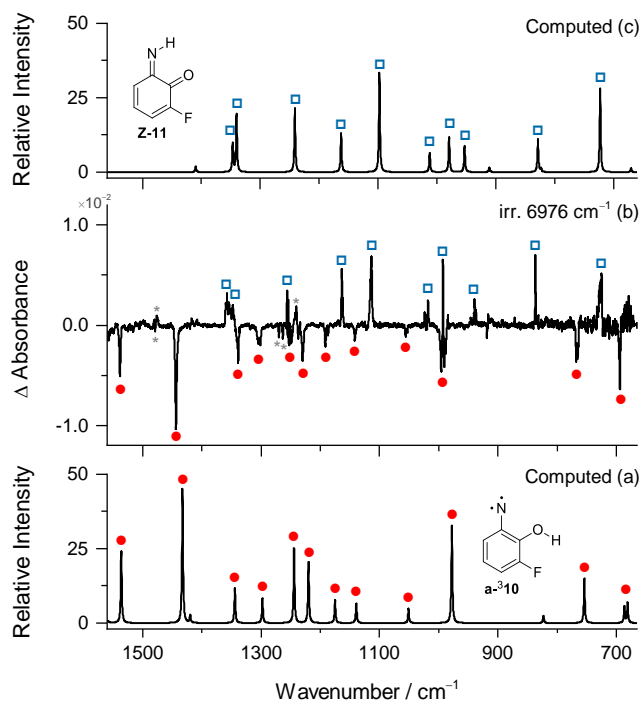

Figure 2. (a) B3LYP/6-311+G(2d,p) computed IR spectrum of triplet *anti*-3-fluoro-2-hydroxyphenylnitrene a-³10. (b) Experimental difference IR spectrum showing changes resulting from irradiation at 6976 cm⁻¹ (60 mW, 1 h), subsequent to irradiation of 9 at λ = 255 nm (Figure S4). The downward bands are due to consumed species assigned to a-³10. The upward bands are due to the produced species assigned to Z-11. Asterisk (∗) indicate minor changes in the population of conformers of 9. (c) B3LYP/6-311+G(2d,p) computed IR spectrum of (Z)-2-fluoro-6-imino-2,4-cyclohexadienone Z-11.

To better understand the "reactive" nature of *syn*-OH nitrene s-³10, the PES around this species was computed (Figure 3). A conceivable mechanism for the reaction of s-³10 is the occurrence of H-atom QMT on the triplet surface to Z-³11, followed by intersystem crossing to Z-11.[52] However, the height (~98.2 kJ mol⁻¹) of the barrier from s-³10 to Z-³11 seems incompatible with the occurrence of a very fast QMT reaction justifying the elusive nature of s-³10; its half-life time would be 1.14 × 10³ s based on the Wentzel−Kramers−Brillouin approximation (see SI). An alternative mechanism for the reaction of s-³10 is the occurrence of H-atom QMT to Z-11 through crossing surfaces from triplet to singlet. To explore this possibility, we searched for a minimum-energy crossing point (MECP) connecting the triplet s-³10 and singlet Z-11 surfaces, first at CASSCF(8,8)/6-31G(d) and then at B3LYP/6-311+G(2d,p) (see SI). Starting with a geometry where the two PESs cross as a function of r(O-H) distance, a global optimization algorithm was employed and an MECP was found with a relative energy of ~39.3 kJ mol⁻¹ at B3LYP/6-311+G(2d,p) + ZPVE (Figure 3). The spin-forbidden H-atom QMT rate was then calculated by non-adiabatic transition state theory (NA-TST) using weak coupling (WC) formulation (see SI).[53] Considering the MECP energy and all additional data from the B3LYP/6-311+G(2d,p) computations, the calculated WC rate constant at 10 K yields for s-³10 an half-life of ~2.60 × 10⁻² s. This indicates that s-³10 reacts promptly by H-atom QMT through crossing triplet to singlet PESs to Z-11, deciphering its reactive and elusive nature.
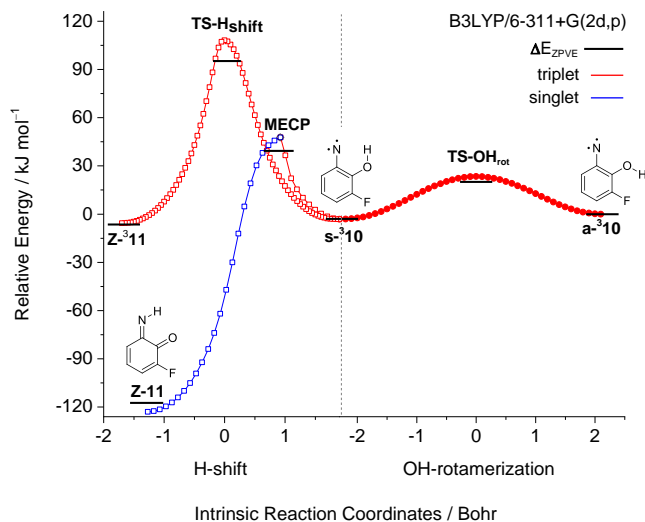
Figure 3. B3LYP/6-311+G(2d,p) computed intrinsic reaction coordinate (IRC) profile for the OH-rotamerization of $^3\mathbf{10}$, for the H-shift of $\mathbf{s}$-$^3\mathbf{10}$ to $\mathbf{Z}$-$^3\mathbf{11}$, and from the MECP connecting $\mathbf{s}$-$^3\mathbf{10}$ and $\mathbf{Z}$-$\mathbf{11}$. For visualization proposes, the IRC curve from the MECP was superimposed on the IRC curve for H-shift and shifted along the horizontal axis so the point corresponding to $\mathbf{s}$-$^3\mathbf{10}$ has the same reaction coordinate in both curves; all the other reaction coordinates represent different structures for each IRC profile. The horizontal bars at each single point (minima, transition states and MECP) show the corresponding computed ZPVE-corrected energy relative to $\mathbf{a}$-$^3\mathbf{10}$.

In conclusion, we demonstrate how to switch on a QMT reaction by conformational control using external radiation. Upon trapping triplet 2-hydroxyphenylnitrene $\mathbf{a}$-$^3\mathbf{10}$ in an N_2 matrix at 10 K, its OH moiety was manipulated (*anti* → *syn*) using vibrational excitation at the $2\nu(OH)$ frequency, moving the H-atom closer to the vicinal nitrene center. Consequently, fast H-atom QMT from $\mathbf{s}$-$^3\mathbf{10}$ to singlet $\mathbf{Z}$-$\mathbf{11}$ was triggered. NA-TST computations unravel that such a reaction occurs through crossing PESs, establishing in this way a rare model for a nonadiabatic H-atom QMT. Overall, our work provides an important conceptual strategy to harness the control of QMT, which will inspire new advances that can extend from enzymatic catalysis[54] to quantum switches.[55]

ASSOCIATED CONTENT

Supporting Information

The Supporting Information is available free of charge on the ACS Publications website.

Experimental and computational procedures, additional experimental results, vibrational assignments, MECP and tunneling rate computations, and computational data (PDF).

AUTHOR INFORMATION

Corresponding Author

*cmnunes@qui.uc.pt

Notes
The authors declare no competing financial interests.

REFERENCES

(1)   Marples, B. A. *Elementary Organic Stereochemistry and Conformational Analysis*; Royal Society of Chemistry: London, 1981.

(2)   Seemann, J. I. Effect of Conformational Change on Reactivity in Organic Chemistry. Evaluations, Applications, and Extensions of Curtin-Hammett Winstein-Holness Kinetics. *Chem. Rev.* **1983**, *83*, 84–130.

(3)   Boehr, D. D.; Nussinov, R.; Wright, P. E. The Role of Dynamic Conformational Ensembles in Biomolecular Recognition. *Nat. Chem. Biol.* **2009**, *5*, 789–796.

(4)   James, L. C.; Roversi, P.; Tawfik, D. S. Antibody Multispecificity Mediated by Conformational Diversity. *Science* **2003**, *299*, 1362–1367.

(5)   Lemouchi, C.; Iliopoulos, K.; Zorina, L.; Simonov, S.; Wzietek, P.; Cauchy, T.; Rodríguez-Fortea, A.; Canadell, E.; Kaleta, J.; Michl, J.; Gindre, D.; Chrysos, M.; Batail, P. Crystalline Arrays of Pairs of Molecular Rotors: Correlated Motion, Rotational Barriers, and Space-Inversion Symmetry Breaking Due to Conformational Mutations. *J. Am. Chem. Soc.* **2013**, *135*, 9366–9376.

(6)   Kudernac, T.; Ruangsupapichat, N.; Parschau, M.; Maciá, B.; Katsonis, N.; Harutyunyan, S. R.; Ernst, K. H.; Feringa, B. L. Electrically Driven Directional Motion of a Four-Wheeled Molecule on a Metal Surface. *Nature* **2011**, *479*, 208–211.

(7)   Murray, B. S.; Menin, L.; Scopelliti, R.; Dyson, P. J. Conformational Control of Anticancer Activity: The Application of Arene-Linked Dinuclear Ruthenium(II) Organometallics. *Chem. Sci.* **2014**, *5*, 2536–2545.

(8)   Kilaj, A.; Gao, H.; Tahchieva, D.; Ramakrishnan, R.; Bachmann, D.; Gillingham, D.; von Lilienfeld, O. A.; Küpper, J.; Willitsch, S. Quantum-Chemistry-Aided Identification, Synthesis and Experimental Validation of Model Systems for Conformationally Controlled Reaction Studies: Separation of the Conformers of 2,3-Dibromobuta-1,3-Diene in the Gas Phase. *Phys. Chem. Chem. Phys.* **2020**, *22*, 13431–13439.

(9)   Zhong, J.; Carignano, M. A.; Kais, S.; Zeng, X. C.; Francisco, J. S.; Gladich, I. Tuning the Stereoselectivity and Solvation Selectivity at Interfacial and Bulk Environments by Changing Solvent Polarity: Isomerization of Glyoxal in Different Solvent Environments. *J. Am. Chem. Soc.* **2018**, *140*, 5535–5543.

(10)   Meana-Pañeda, R.; Fernández-Ramos, A. Tunneling and Conformational Flexibility Play Critical Roles in the Isomerization Mechanism of Vitamin D. *J. Am. Chem. Soc.* **2012**, *134*, 346–354.

(11)   Chang, Y. P.; Długołêcki, K.; Küpper, J.; Rösch, D.; Wild, D.; Willitsch, S. Specific Chemical Reactivities of Spatially Separated 3-Aminophenol Conformers with Cold Ca^+ Ions. *Science* **2013**, *342*, 98–101.

(12)   Bhattacharya, A.; Shin, J. W.; Clawson, K. J.; Bernstein, E. R. Conformation Specific and Charge Directed Reactivity of Radical Cation Intermediates of α-Substituted (Amino, Hydroxy, and Keto) Bioactive Carboxylic Acids. *Phys. Chem. Chem. Phys.* **2010**, *12*, 9700–9712.

(13)   Kim, M. H.; Shen, L.; Tao, H.; Martinez, T. J.; Suits, A. G. Conformationally Controlled Chemistry: Excited-State Dynamics Dictate Ground-State Reaction. *Science* **2007**, *315*, 1561–1565.

(14)   Zuev, P. S.; Sheridan, R. S.; Sauers, R. R.; Moss, R. A.; Chu, G. Conformational Product Control in the Low-Temperature Photochemistry of Cyclopropylcarbenes. *Org. Lett.* **2006**, *8*, 4963–4966.

(15)   Khriachtchev, L.; Maçôas, E.; Pettersson, M.; Räsänen, M. Conformational Memory in Photodissociation of Formic Acid. *J. Am. Chem. Soc.* **2002**, *124*, 10994–10995.

(16)   Park, S. T.; Kim, S. K.; Kim, M. S. Observation of Conformation-Specific Pathways in the Photodissociation of 1-Iodopropane Ions. *Nature* **2002**, *415*, 306–308.

(17)   Nunes, C. M.; Reva, I.; Fausto, R. Direct Observation of Tunnelling Reactions by Matrix Isolation Spectroscopy. In *Tunnelling in Molecules: Nuclear Quantum Effects from Bio to Physical Chemistry*; The Royal Society of Chemistry, 2021; pp 1–60.

(18)   Schreiner, P. R. Quantum Mechanical Tunneling is Essential to Understanding Chemical Reactivity. *Trends Chem.* **2020**, *2*, 980–989.

(19)   Borden, W. T. Reactions That Involve Tunneling by Carbon and the Role that Calculations Have Played in Their Study. *Wiley Interdiscip. Rev. Comput. Mol. Sci.* **2016**, *6*, 20–46.

(20)   Bell, R. P. *The Tunnel Effect in Chemistry*; Springer: Boston, MA, 1980.

(21)   Kozuch, S.; Zhang, X.; Hrovat, D. A.; Borden, W. T. Calculations on Tunneling in the Reactions of Noradamantyl Carbenes. *J. Am. Chem. Soc.* **2013**, *135*, 17274–17277.

(22)   Mardyukov, A.; Quanz, H.; Schreiner, P. R. Conformer-Specific Hydrogen Atom Tunnelling in Trifluoromethylhydroxycarbene. *Nat. Chem.* **2017**, *9*, 71–76.

(23)   Eckhardt, A. K.; Erb, F. R.; Schreiner, P. R. Conformer-Specific [1,2]H-Tunnelling in Captodatively-Stabilized Cyanohydroxycarbene (NC-C-OH). *Chem. Sci.* **2019**, *10*, 802–808.

(24)   Nunes, C. M.; Viegas, L. P.; Wood, S. A.; Roque, J. P. L.; McMahon, R. J.; Fausto, R. Heavy-Atom Tunneling Through Crossing Potential Energy Surfaces: Cyclization of a Triplet 2-Formylarylnitrene to a Singlet 2,1-Benzisoxazole. *Angew. Chem. Int. Ed.* **2020**, *59*, 17622–17627.

(25)   Nunes, C. M.; Knezz, S. N.; Reva, I.; Fausto, R.; McMahon, R. J. Evidence of a Nitrene Tunneling Reaction: Spontaneous Rearrangement of 2-Formyl Phenylnitrene to an Imino Ketene in Low-Temperature Matrixes. *J. Am. Chem. Soc.* **2016**, *138*, 15287–15290.

(26)   Schleif, T.; Mieres-Perez, J.; Henkel, S.; Mendez-Vega, E.; Inui, H.; McMahon, R. J.; Sander, W. Conformer-Specific Heavy-Atom Tunneling in the Rearrangement of Benzazirines to Ketenimines. *J. Org. Chem.* **2019**, *84*, 16013–16018.

(27)   Another possible case of conformational structure influence on heavy-atom QMT occurs in the ring-expansion of *exo*-1-methylcyclobutylfluorocarbene to the corresponding cyclopentene in a nitrogen matrix at 8 K, with the *endo*-conformer being unreactive under the same conditions (although both conformers were found to react at 16 K or in a argon matrix). See: Zuev, P. S.; Sheridan, R. S.; Albu, T. V.; Truhlar, D. G.; Hrovat, D. A.; Borden, W. T. Carbon Tunneling from a Single Quantum State. *Science* **2003**, *299*, 867–870.

(28)   Klinman, J. P.; Kohen, A. Hydrogen Tunneling Links Protein Dynamics to Enzyme Catalysis. *Annu. Rev. Biochem.* **2013**, *82*, 471–496.

(29)   Klinman, J. P. An Integrated Model for Enzyme Catalysis Emerges from Studies of Hydrogen Tunneling. *Chem. Phys. Lett.* **2009**, *471*, 179–193.

(30)   Offenbacher, A. R.; Sharma, A.; Doan, P. E.; Klinman, J. P.; Hoffman, B. M. The Soybean Lipoxygenase-Substrate Complex: Correlation between the Properties of Tunneling-Ready States and ENDOR-Detected Structures of Ground States. *Biochemistry* **2020**, *59*, 901–910.

(31)   Horitani, M.; Offenbacher, A. R.; Marcus Carr, C. A.; Yu, T.; Hoeke, V.; Cutsail, G. E.; Hammes-Schiffer, S.; Klinman, J. P.; Hoffman, B. M. [13]C ENDOR Spectroscopy of Lipoxygenase-Substrate Complexes Reveals the Structural Basis for C-H Activation by Tunneling. *J. Am. Chem. Soc.* **2017**, *139*, 1984–1997.

(32)   Hu, S.; Sharma, S. C.; Scouras, A. D.; Soudackov, A. V.; Carr, C. A. M.; Hammes-Schiffer, S.; Alber, T.; Klinman, J. P. Extremely Elevated Room-Temperature Kinetic Isotope Effects Quantify the Critical Role of Barrier Width in Enzymatic C-H Activation. *J. Am. Chem. Soc.* **2014**, *136*, 8157–8160.

(33)   Meyer, M. P.; Tomchick, D. R.; Klinman, J. P. Enzyme Structure and Dynamics Affect Hydrogen Tunneling: The Impact of a Remote Side Chain (I553) in Soybean Lipoxygenase-1. *Proc. Natl. Acad. Sci. U. S. A.* **2008**, *105*, 1146–1151.

(34)   For examples of conformational isomerization QMT reactions directly observed by matrix isolation spectroscopy see ref. 17. See also:

Ogruc Ildiz, G.; Fausto, R. Structural Aspects of the Ortho Chloro- and Fluoro-Substituted Benzoic Acids: Implications on Chemical Properties. *Molecules* **2020**, *25*, 4908.

(35)   Interestingly, Quack *et al*. developed theoretically a molecular quantum switch (*meta*-deuterium-phenol), which can operate by coherent IR excitation and having a readout process associated with the OH conformational change. See: Fábri, C.; Albert, S.; Chen, Z.; Prentner, R.; Quack, M. A Molecular Quantum Switch Based on Tunneling in *meta*-D-Phenol C_6H_4DOH. *Phys. Chem. Chem. Phys.* **2018**, *20*, 7387–7394.

(36)   Morawietz, J.; Sander, W. Matrix Isolation of o-Quinoid Compounds - 6-Imino-2,4-Cyclohexadien-1-One and 1,2-Diimino-3,5-Cyclohexadiene. *Liebigs Ann.* **1996**, *2029*–2037.

(37)   Tomioka, H.; Matsushita, T.; Murata, S.; Koseki, S. Photochemistry of Phenyl Azides Bearing 2-Hydroxy and 2-Amino Groups Studied by Matrix-Isolation Spectroscopy: Generation and Characterization of Reactive o-Quinoid Compounds. *Liebigs Ann.* **1996**, 1971–1980.

(38)   In this sense, **s-[3]10'** is a case of a molecular system that is characterized by "quantum tunneling instability", a concept that has been recently proposed by Kozuch *et al*. See: Amlani, H.; Frenklah, A.; Kozuch, S. Chapter 2 Tunnelling Instability in Molecular Systems. An Exercise in Computational Chemistry Prediction Power. In *Tunnelling in Molecules: Nuclear Quantum Effects from Bio to Physical Chemistry*; The Royal Society of Chemistry, 2021; pp 61–87.

(39)   Olivucci, M.; Santoro, F. Chemical Selectivity through Control of Excited-State Dynamics. *Angew. Chem. Int. Ed.* **2008**, *47*, 6322–6325.

(40)   The selective irradiation of the *syn*-OH conformer **as-9** at its OH stretching overtone (6938 cm^{-1}) confirms that the v(OH) and 2v(OH) bands observed at higher frequencies belong to distinct *anti*-OH conformers (Figure S2). Such experiment led to the selective conversion of **as-9** [e.g., the v(OH) band at 3573 cm^{-1} decreases] into the *anti*-OH conformer **aa-9** [e.g., the v(OH) band centered at ~3591 cm^{-1} increases], while the *anti*-OH conformer **sa-9** remained unchanged [e.g., the v(OH) band at 3603 cm^{-1} does not change].

(41)   Essentially all **a-[3]10** is preserved under dark conditions (≥98%) on the experimental time scale of ~1 h, whereas more than half of it is consumed upon near-IR irradiation as described further in the text. An eventual slow decay of **a-[3]10** in an N_2 matrix in the dark at 10 K is under investigation.

(42)   Lopes Jesus, A. J.; Nunes, C. M.; Fausto, R.; Reva, I. Conformational Control over an Aldehyde Fragment by Selective Vibrational Excitation of Interchangeable Remote Antennas. *Chem. Commun.* **2018**, *54*, 4778–4781.

(43)   Schanz, R.; Boţan, V.; Hamm, P. A Femtosecond Study of the Infrared-Driven *cis-trans* Isomerization of Nitrous Acid (HONO). *J. Chem. Phys.* **2005**, *122*, 044509.

(44)   Dian, B. C.; Longarte, A.; Zwier, T. S. Conformational Dynamics in a Dipeptide after Single-Mode Vibrational Excitation. *Science* **2002**, *296*, 2369–2373.

(45)   Pettersson, M.; Lundell, J.; Khriachtchev, L.; Räsänen, M. IR Spectrum of the Other Rotamer of Formic Acid, *cis*-HCOOH. *J. Am. Chem. Soc.* **1997**, *119*, 11715–11716.

(46)   Fausto, R.; Khriachtchev, L.; Hamm, P. Conformational Changes in Cryogenic Matrices. In *Physics and Chemistry at Low Temperatures*; Khriachtchev, L., Ed.; Pan Stanford Publishing: United States, 2011; pp 51–84.

(47)   Nunes, C. M.; Reva, I.; Fausto, R. Conformational Isomerizations Triggered by Vibrational Excitation of Second Stretching Overtones. *Phys. Chem. Chem. Phys.* **2019**, *21*, 24993–25001.

(48)   Lopes Jesus, A. J.; Nunes, C. M.; Reva, I.; Pinto, S. M. V.; Fausto, R. Effects of Entangled IR Radiation and Tunneling on the Conformational Interconversion of 2-Cyanophenol. *J. Phys. Chem. A* **2019**, *123*, 4396–4405.

(49)   Maçôas, E. M. S.; Khriachtchev, L.; Pettersson, M.; Juselius, J.; Fausto, R.; Räsänen, M. Reactive Vibrational Excitation Spectroscopy of Formic Acid in Solid Argon: Quantum Yield for Infrared Induced *trans→cis* Isomerization and Solid State Effects on the Vibrational Spectrum. *J. Chem. Phys.* **2003**, *119*, 11765–11772.

(50)   This transformation was not induced when irradiations were performed at random frequencies outside the 6976–7000 cm^{-1} range.

(51)   As shown further in the text, there is no available reaction path connecting **a-[3]10** with **Z-11** other than through **s-[3]10**, which must involve crossing the triplet to singlet potential energy surfaces (a spin forbidden process). The direct formation of **Z-11** upon vibrational excitation of **a-[3]10** is impossible in practice, since it cannot compete with the vibrational relaxation leading to **s-[3]10** that must occur on the time scale of ps.

(52)   A similar mechanism was proposed to explain the observation of H-atom QMT of triplet nitrene **a**-^{3}**3** to imino-ketene **4** (Scheme 1; ref. 25). See also: Liu, J.; Wu, Z.; Yang, Y.; Qian, W.; Wang, L.; Zeng, X. 3-Nitrene-2-Formylthiophene and 3-Nitrene-2-Formylfuran: Matrix Isolation, Conformation, and Rearrangement Reactions. *J. Phys. Chem. A* **2020**, *124*, 3786–3794.

(53)   The WC formulation of NA-TST has been recently found to provide rate constants in fair agreement with experimental measurements for a couple of spin-forbidden heavy-atom QMT cyclizations that were directly observed under cryogenic conditions (ref. 24). See also: Viegas, L. P.; Nunes, C. M.; Fausto, R. Spin-Forbidden Heavy-Atom Tunneling in the Ring-Closure of Triplet Cyclopentane-1,3-Diyl. *Phys. Chem. Chem. Phys.* **2021**, *23*, 5797–5803.

(54)   Layfield, J. P.; Hammes-Schiffer, S. Hydrogen Tunneling in Enzymes and Biomimetic Models. *Chem. Rev.* **2014**, *114*, 3466–3494.

(55)   Litman, Y.; Rossi, M. Multidimensional Hydrogen Tunneling in Supported Molecular Switches: The Role of Surface Interactions. *Phys. Rev. Lett.* **2020**, *125*, 216001.

1
2
3
4
5
6
7
8
9
10
11
12
13
14
15
16
17
18
19
20
21
22
23
24
25
26
27
28
29
30
31
32
33
34
35
36
37
38
39
40
41
42
43
44
45
46
47
48
49
50
51
52
53
54
55
56
57
58
59
60

6

Table of Contents (TOC)
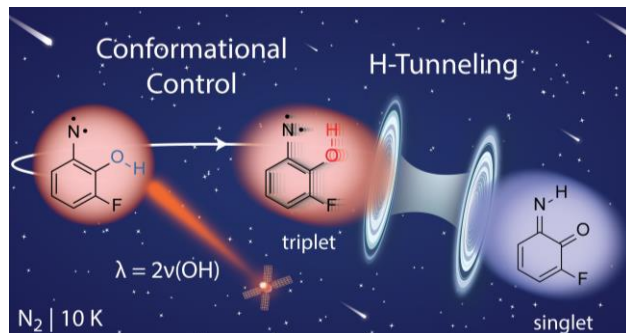
Supporting Information (SI)

Switching on H-tunneling through conformational control

José P. L. Roque,[1] Cláudio M. Nunes,[1]* Luís P. Viegas,[1] Nelson A. M. Pereira,[1] Teresa M. V. D. Pinho e Melo,[1] Peter R. Schreiner,[2] and Rui Fausto[1]

[1]University of Coimbra, CQC, Department of Chemistry, 3004-535 Coimbra, Portugal

[2]Institute of Organic Chemistry, Justus Liebig University, Heinrich-Buff-Ring 17, 35392 Giessen, Germany

TABLE OF CONTENTS

1. Experimental and Computational Methods

Synthesis of 3-fluoro-2-hydroxyphenylazide 9

General: Commercial reagents were used as purchased. ^{1}H and ^{13}C Nuclear Magnetic Resonance (NMR) spectra were recorded on an NMR spectrometer Bruker Avance III operating at 400 and 100 MHz, respectively. Chemical shifts are referred to the residual signal of DMSO‑d_6, ^{1}H NMR ($\delta_H = 2.50$) and ^{13}C NMR ($\delta_C = 39.5$), or to the internal standard tetramethylsilane (TMS). Chemical shifts are given in parts per million (ppm) relative to TMS and coupling constants J are given in Hertz. Thin-layer chromatography (TLC) was carried out on silica gel 60 F_{254} plates (AL TLC 20 × 20). Column chromatography was performed on Silica Gel 60 (0.04 − 0.063 mm). High-resolution mass spectra (HRMS) were obtained with a Waters Micromass VG Autospec M ESI-TOF spectrometer.

Synthesis: The synthesis of 3-fluoro-2-hydroxyphenylazide **9** (Scheme S1) was carried out based on a procedure described in the literature for the preparation of other azidophenol derivatives.[1]
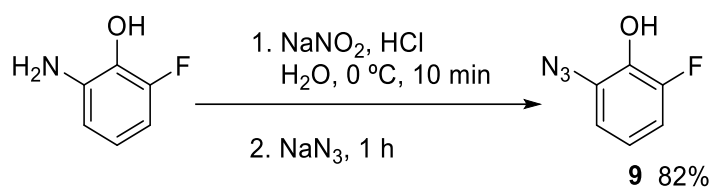
Scheme S1. Synthesis of 3-fluoro-2-hydroxyphenylazide **9**.

Concentrated HCl (37% v/v, 1.1 mL) was added dropwise to a suspension of 2-amino-6-fluorophenol (0.5 g, 3.9 mmol) in water (12.5 mL), at 0 °C, followed by the addition of a solution of NaNO$_2$ (0.27 g, 3.9 mmol, 1 eq) in water (1.2 mL). After 10 min, the cooling bath was removed and the reaction mixture was allowed to warm to room temperature. Sodium azide (0.31 g, 4.8 mmol and 1.2 eq) was added portionwise and, after stirring at room temperature for 1 h, the reaction mixture was extracted with EtOAc (25 mL), the organic layer washed with brine (25 mL), water (25 mL) and dried over anhydrous sodium sulphate. The solvent was removed by evaporation followed by purification of the crude product by flash chromatography [ethyl acetate/hexane (1:2)]. The azide **9** was obtained as a light brown solid in 82% yield (0.49 g, 3.2 mmol).

Characterization of **9**: ^{1}H NMR (400 MHz, DMSO-d$_6$): δ (ppm) 10.21 (bs, 1H, OH), 7.04-6.97 (m, 1H, Ph-H), 6.86-6.79 (m, 2H, Ph-H). ^{13}C NMR (100 MHz, DMSO-d$_6$): δ (ppm) 151.9 (d, J_{CF} =239.5 Hz), 138.1 (d, J_{CF} = 16.7 Hz), 128.6 (d, J_{CF} = 4.8 Hz), 119.4 (d, J_{CH} = 8.4 Hz), 116.3 (d, J_{CH} = 2.7 Hz), 112.6 (d, J_{CH} = 18.8 Hz). HRMS (ESI$^+$, m/z) calcd for $C_6H_4FN_3ONa$ (M+Na)$^+$ = 176.0231, found 176.0232.

Matrix Isolation IR Spectroscopy: A sample of 3-fluoro-2-hydroxyphenylazide **9** was placed in a glass tube, which was then connected to a closed-cycle helium cryostat (Advanced Research Systems DE-202) through a stainless-steel needle valve (SS-4BMRG NUPRO). Possible traces of volatile impurities were removed by pumping the sample through the cryostat at room temperature. Monomeric matrices were prepared by co-deposition of vapors of **9** at room temperature and a large excess of nitrogen gas (N50, Air Liquide) onto a cold (10 K) CsI optical substrate. The temperature of the CsI window was directly measured by a silicon diode, connected to a digital controller (LakeShore 311), and stabilized with an accuracy of 0.1 K.

Infrared spectra were recorded using a Thermo Nicolet 6700 Fourier transform infrared (FTIR) spectrometer, equipped with a Mercury Cadmium Telluride (MCT-B) detector (cooled with liquid nitrogen) and a KBr beam splitter, for the mid-IR range (4000–400 cm^{-1}), or a Indium Gallium Arsenide (InGaAs) detector and a CaF$_2$ beam splitter, for the near-IR range (7500–4000 cm^{-1}). When there was the need to protect the sample from part of the infrared light, the mid-IR spectra were collected in the range 1580–400 cm^{-1} by using a long-pass filter (Spectrogon LP-6300 nm, transmission cut-off value ~1587 cm^{-1}) placed between the spectrometer light source and the sample. The infrared spectra were recorded with resolution 0.5 or 2 cm^{-1} in the mid-IR and near-IR ranges, respectively. To reduce the interference from atmospheric H_2O and CO_2, a stream of dry and CO_2 filtered-off air was used to continuously purge the optical path of the spectrometer.

UV and Near-IR Irradiation Experiments: The matrix-isolated species were irradiated through the outer KBr window of the cryostat using a frequency-tunable narrowband light [full width at half-maximum (fwhm) of ~0.2 cm^{-1}] generated by a frequency-doubled signal (UV range) or an idler (near-IR range) beam of an optical parametric oscillator (Spectra Physics Quanta-Ray MOPO-SL) pumped with a pulsed Nd:YAG laser (Spectra-Physics PRO-230: output power ~4.4 W; wavelength = 355 nm; duration = 10 ns; repetition rate = 10 Hz).

IR Spectra and Thermochemistry Computations: The geometry optimizations and harmonic frequency computations were performed for the most relevant stationary points of **9**, **9'**, **10**, and **11** at the B3LYP/6-311+G(2d,p) level of theory,[2–5] using the Gaussian 16 software package.[6] All computations were performed using tight optimization criteria. The nature of each stationary point was inspected by the analysis of the Hessian matrices. To take into consideration the neglected anharmonic effects, the limitations of the implemented methods and the limitations of the basis set, the harmonic vibrational frequencies were scaled by a factor of 0.979 or 0.955 for wavenumbers above or below 2500 cm^{-1}, respectively.[7] The scaled harmonic vibrational frequencies and respective absolute intensities were used to simulate the IR spectra by convoluting each peak with a Lorentzian function having an fwhm of 2 cm^{-1}. Anharmonic frequency computations for **9** and **a**-^{3}**10** were carried out at the B3LYP/6-311+G(2d,p) level of theory, using the fully automated generalized second-order vibrational perturbative theory (GVPT2), as implemented in Gaussian 16.[8–10] Thermochemistry computations for **9** and **9'** were carried out at the B3LYP/6-311+G(2d,p) and CBS-QB3[11,12] levels of theory. The computed data were then used to estimate the relative Gibbs energy at 298.15 K (ΔG_{298K}) for the different conformers and their room temperature Boltzmann populations.

Normal mode analysis: The theoretical normal modes of **a**-^{3}**10** and **Z-11** were analyzed by carrying out potential energy distribution (PED) calculations. The calculated force constants with respect to Cartesian coordinates, obtained from the Gaussian 16 computations, were transformed into the force constants with respect to internal coordinates, which allowed the PED analysis to be carried out as described elsewhere.[13] The set of internal coordinates used for **a**-^{3}**10** and **Z-11** were defined as recommended by Pulay *et al.*[14] and are given in Tables S2 and S3, respectively. The atom numberings of **a**-^{3}**10** and **Z-11,** used for the definition of the internal coordinates, are shown in Figure S5. The vibrational assignment of **a**-^{3}**10** and **Z-11** and the obtained PED matrices are presented in Tables S4 and S5, respectively.

MECP Computations: Due to the open-shell nature of the nitrene species, the potential energy surface (PES) connecting **a**-^{3}**10** and **Z-11** was preliminarily screened at the multiconfigurational CASSCF(8,8)/6-31G(d) level of theory using the Gaussian 16 software package.[6] An eight electron- eight orbital (8,8) complete active space (CAS) was used for all species. For nitrene **10**,

the defined CAS consists of seven out-of-plane π/π^* orbitals (A") and one in-plane p atomic orbital (A') (Figure S6).[15] We computed the minimum corresponding to two conformers of the triplet ground-state (TGS) nitrene (**a**-^{3}**10** and **s**-^{3}**10**), two conformers of the open-shell singlet (OSS) nitrene (**a**-^{OSS}**10** and **s**-^{OSS}**10**), and one conformer of the closed-shell singlet (CSS) nitrene (**a**-^{CSS}**10**). The putative **s**-^{CSS}**10** conformer, with a OH group facing the reactive nitrene center could not be located as a minimum. For the imino **Z**-**11**, the defined CAS consists of eight out-of-plane π/π^* orbitals (A") (Figure S6). We computed the minimum corresponding to the singlet ground-state imino (**Z**-**11**) and to triplet state imino (**Z**-^{3}**11**).

The nitrene **s**-^{3}**10** and imino **Z**-**11** have different ground state multiplicities (triplet and singlet) and, therefore, the existence of a minimum-energy crossing point (MECP) connecting both species was investigated. An initial MECP search was performed using the so-called partial optimization method. In this case, by running relaxed PES scans as a function of the r(OH) coordinate (i.e., optimizing all internal coordinates while incrementally fixing the OH bond distance), starting from the minima found before; **s**-^{3}**10**, **s**-^{OSS}**10**, **Z**-**11**, and **Z**-^{3}**11** (Figure S7). The increment used between each scan step was 0.02 Å (regarding the OH bond distance), a small value to avoid discontinuities in the active space. The partial optimization method is a modest approximation for the search of a MECP because all the coordinates except the r(OH) are optimized separately in each surface, rather than converging together.[16,17] Nonetheless, this approach provides useful insights into the PES investigated. First, it shows the dissociative character of the **s**-^{CSS}**10** (^{1}A') surface along the r(OH) coordinate as connecting to singlet **Z**-**11**, thus explaining the lack of success in finding the **s**-^{CSS}**10** minimum. Second, it shows that **s**-^{OSS}**10** (^{1}A") surface is parallel to **s**-^{3}**10** (^{3}A") surface, and therefore, the existence of a MECP between these surfaces is unlikely. Finally, it shows that it is likely that there exists an MECP at the crossing between the triplet A" and CSS A' surfaces, directly connecting **s**-^{3}**10** and **Z**-**11**. A subsequent full MECP search was performed using a global optimization algorithm employing the EasyMECP software package,[18] which is a python script developed based on the work of Harvey et al.[19] This software was used as default, requiring solely the inclusion of an energy-parse code to allow reading the data of CASSCF computations performed in Gaussian 16. The structure on the singlet surface previously obtained by the partial optimization method, near the crossing between triplet A" and CSS A' surfaces, was used as the input geometry. The initial guess active space orbitals of the input structure at triplet and singlet multiplicities were those of the active space orbitals of

a-^{3}**10** and **Z**-**11**, respectively. Using this method, one MECP was found. Vibrational analysis on the seam of the MECP was carried out using the GLOWfreq software package.[20] Here, two Hessian matrices obtained on each of the diabatic surfaces are combined in one effective Hessian. Then the motion orthogonal to the crossing seam is projected out and the effective Hessian is finally diagonalized to provide the effective vibrational frequencies of the MECP. Finally, intrinsic reaction coordinate (IRC) computations with each multiplicity were performed by following the steepest descendent path from the optimized MECP structure, which confirms that the found MECP connects **a**-^{3}**10** and **Z**-**11**.

To properly account for dynamic electron correlation and to obtain more reliable energies, CASSCF computations are usually augmented by single point computations using a method such as CASPT2. However, the geometry of an MECP can be extremely dependent on the level of theory. Because the MECP depends on the relative positions of two surfaces, changing the level of theory from CASSCF to CASPT2 for performing single point calculations can shift the surfaces relative to one another and lead to unreliable energy values.[19,21] Alternatively, one can perform the MECP search using a time affordable computational method that already includes dynamic electron correlation such as DFT, as long as the method chosen is adequate for the system being studied (e.g., the species to be computed do not possess multiconfigurational character). The need to use multiconfigurational methods for a correct description of most nitrenes species is mainly because of their OSS states.[22] Triplet ground-state arylnitrenes, such as the **s**-^{3}**10**, are properly and reliably described by DFT computations. The product **Z**-**11** is a closed-shell singlet system and there is no need for using multiconfigurational computations. Since the MECP found during the CASSCF search is at the crossing between a triplet and a singlet surface, connecting the **s**-^{3}**10** and **Z**-**11**, it is reasonable to assume that this MECP can be correctly described by DFT methods. Thus, we performed B3LYP/6-311+G(2d,p) relaxed PES scans along the r(OH) coordinate and obtained qualitatively identical results to those performed at the CASSCF level (compare Figures S7 and S8). Accordingly, the partial optimization method carried out at the B3LYP level also suggests the existence of an MECP at a crossing between the triplet A″ and CSS A′ surfaces, connecting the **s**-^{3}**10** and **Z**-**11** species. A subsequent full MECP search was performed at the B3LYP/6-311+G(2d,p) level, according to the method described above for the similar search performed at the CASSCF(8,8)/6-31G(d) level. Additional details are provided in the main text.

Tunneling Rate Computations: The transformation of triplet **s-^{3}10** to singlet **Z-11** is a spin-forbidden reaction involving H-atom tunneling. Two different mechanisms can be envisioned: (i) A two-step mechanism involving an H-atom QMT on the triplet surface from **s-^{3}10** to **Z-^{3}11** followed by intersystem crossing (ISC) to singlet ground state **Z-11**; (ii) A single-step mechanism involving an H-atom QMT through crossing triplet and single surfaces from ^{3}**10** to **Z-11**.

(i) The H-atom QMT rate on the triplet surface (first hypothesis) was computed by the Wentzel-Kramers-Brillouin (WKB) approximation.[23–25] According to this model, the probability *P(E)* of tunneling is given by:

$$P(E) \ = \ e^{-\pi^2 w \sqrt{2m(V_0-E)}/h}, \tag{1.1}$$

where m is the mass of the particle tunneling through a barrier with height V_0 and width w, (V_0-E) is the energy difference of the particle E with respect to the top of the barrier, and h is Planck's constant. Tunneling rates are given by the product of the tunneling probability and the frequency of attempts (i.e., the frequency of the normal mode associated to the reaction coordinate). To obtain the parameters of the barrier, intrinsic reaction coordinate (IRC) profiles connecting **s-^{3}10** to **Z-^{3}11** were computed at the B3LYP/6-311+G(2d,p). The strictly electronic energy profiles were then corrected by the zero-point vibrational energy of the stationary points. After this procedure, the relative barrier height (V_0-E) was computed to be 98.2 kJ mol^{-1} and the barrier width w to be 2.10 bohr (Figure S9). Using equation 1.1, the tunneling probability was estimated to be 1.49×10^{-17}. Considering the computed δ(OH) = 1361 cm^{-1} of **s-^{3}10** as the frequency of attempts, the tunneling rate was estimated to be 6.07×10^{-4} s^{-1} (half-life of 1.14×10^3 s).

(ii) The H-atom QMT rate through crossing triplet and singlet surfaces (second hypothesis) was computed with the weak coupling (WC)[26–28] formulation of non-adiabatic transition state theory (NA-TST),[26,29–34] which we have employed very recently for the calculation of spin-forbidden QMT rate constants.[21,35] The reader is referred to those papers for a detailed description of the procedure. By running the GLOWfreq code with data obtained from B3LYP/6-311+G(2d,p) computations (see above), we obtain the quantities required by the NA-TST equation such as the norm of the difference of the gradients on the two surfaces at the MECP (1.26×10^{-1} hartree bohr^{-1}), the geometric mean of the norms of the mentioned gradients (4.05×10^{-2} hartree bohr^{-1}), the zero-point energy at the MECP (0.0840 hartrees, which leads to an MECP barrier of ~42.1 kJ mol^{-1} relative to **s-^{3}10** [~39.3 kJ mol^{-1} relative to **a-^{3}10**]) and the reduced mass of the mode orthogonal to the crossing seam surface (11.2 amu). However, as suggested by Harvey,[29] we can

expect that in the deep tunneling regime of this particular reaction, the process of breaking an O-H bond and forming an N-H bond will be dominated by the motion of the hydrogen atom alone. Therefore, instead of using 11.2 amu for the reduced mass, we have used a value of 1 amu. The spin-orbit coupling, which also enters the NA-TST equation, was calculated at the B3LYP/6-311+G(2d,p) level with MolSOC [36–38] and found to be 21.17 cm^{-1}. With these data, the NA-TST rate constant at 10 K yields 26.7 s^{-1} (half-life of 0.026 s).

2. Figures
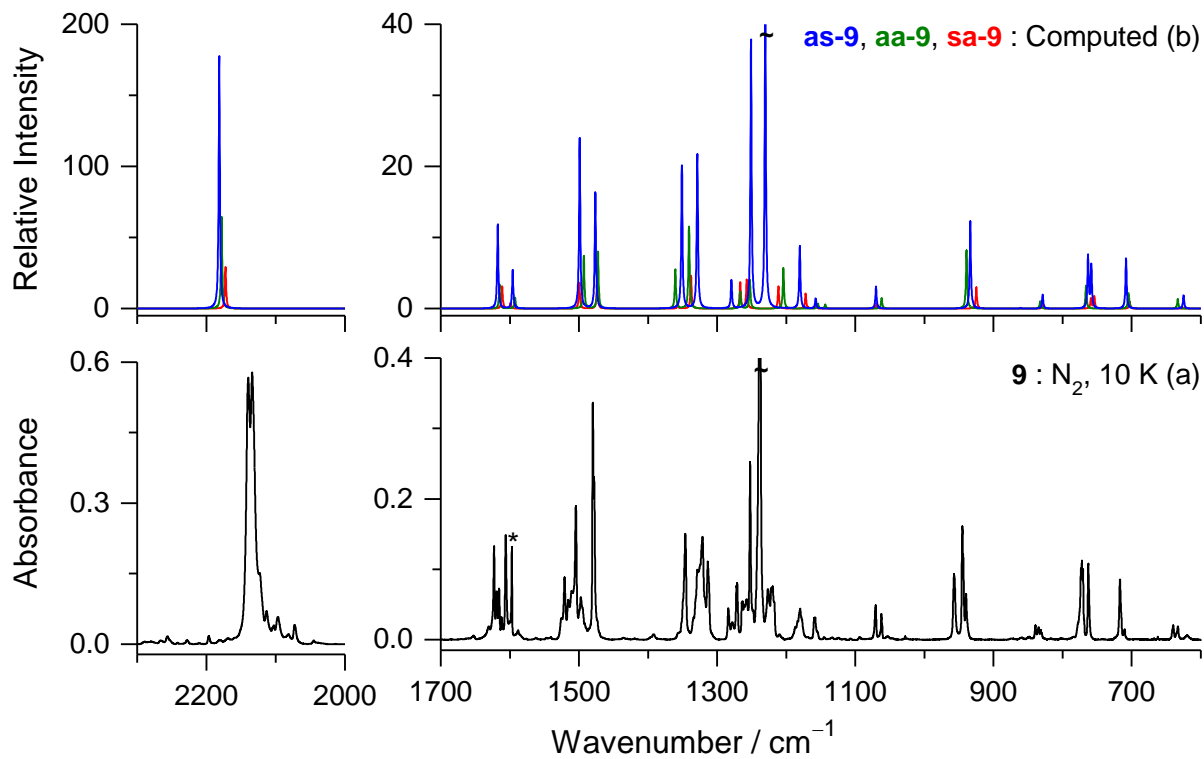
Figure S1. (a) Experimental IR spectrum of 3-fluoro-2-hydroxyphenylazide **9** in a nitrogen matrix at 10 K. The asterisk symbol indicates contribution from monomeric water. (b) IR spectrum of **9** computed at the B3LYP/6-311+G(2d,p) level of theory considering the population of **as-9**, **aa-9** and **sa-9** conformers in a ratio of 66:11:23 (see Table S1).
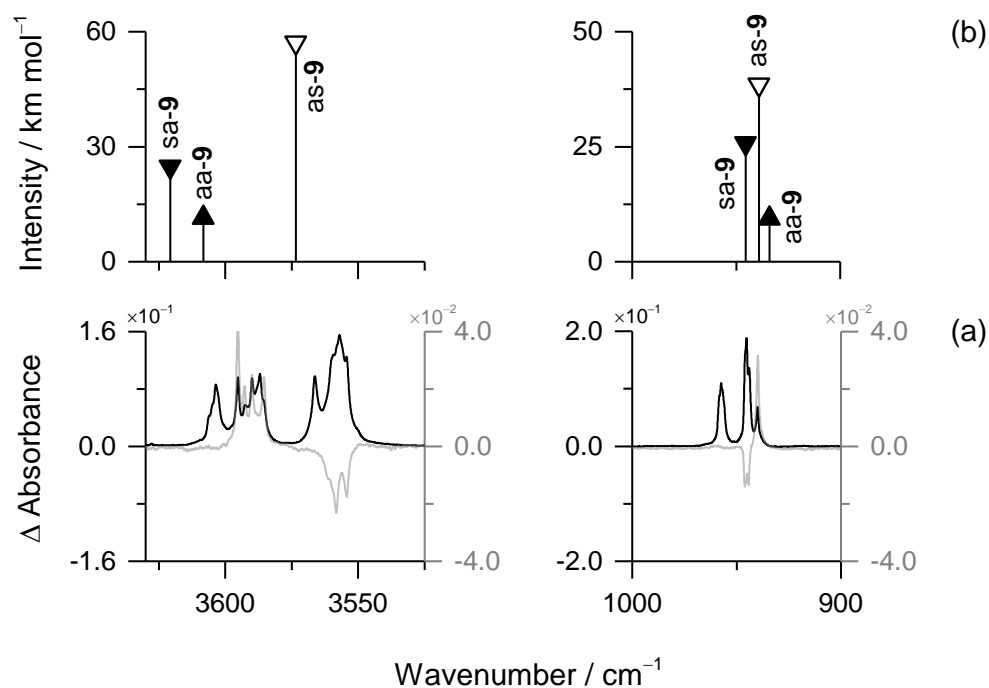
Figure S2. (a) Selected regions showing the mid-IR spectrum collected immediately after the deposition of 3-fluoro-2-hydroxyphenylazide **9** in a nitrogen matrix at 10 K (back line) and the corresponding difference IR spectrum resulting from irradiation at 6938 cm^{-1} (60 mW, 1 h) (gray line). Negative bands indicate the consumption of **as-9** and positive bands the production of **aa-9**. The conformer **sa-9** remains unchanged. (b) Anharmonic wavenumbers and IR intensities computed at the B3LYP/6-311+G(2d,p) level for the **as-9**, **aa-9** and **sa-9** conformers, considering the population ratio of 66:11:23, respectively.
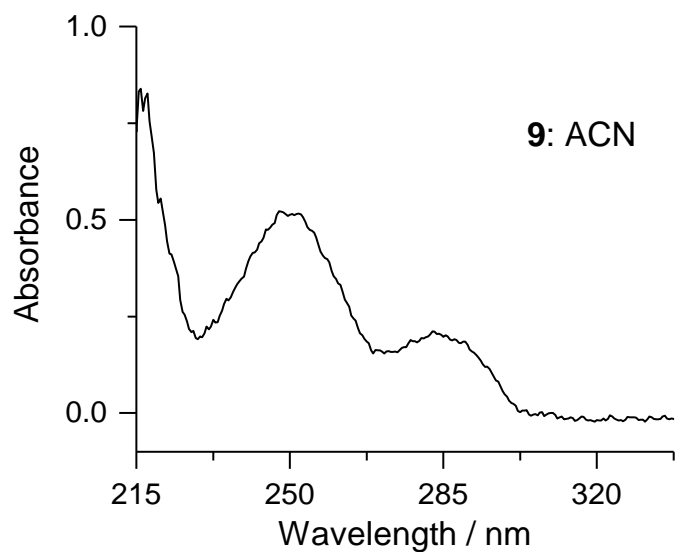
Figure S3. UV-Vis spectrum of 3-fluoro-2-hydroxyphenylazide (**9**) in acetonitrile (ACN). The spectrum was recorded in a Shimadzu UV2501-PC at room temperature.
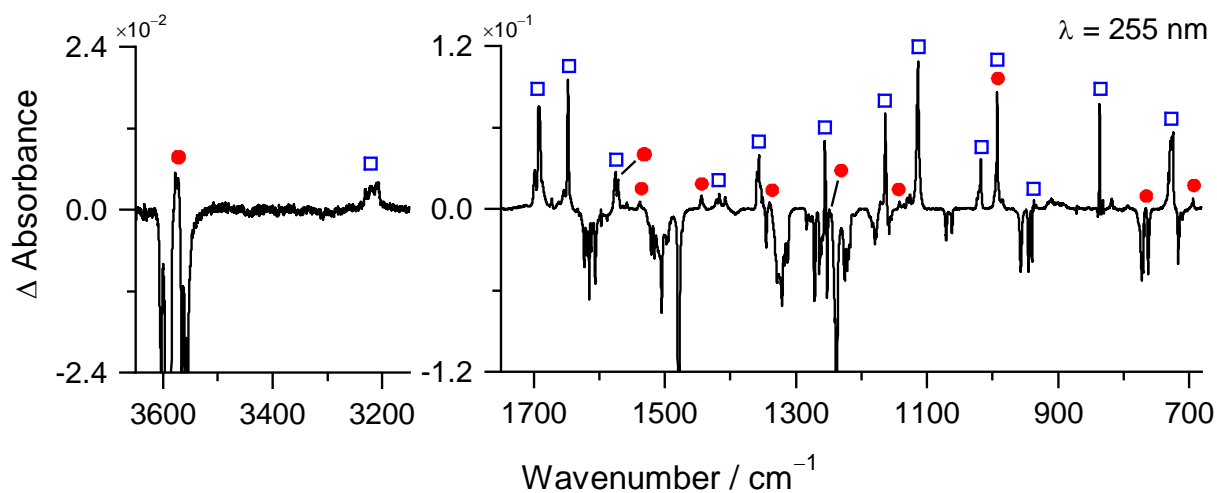
Figure S4. Experimental difference IR spectrum showing changes after irradiation of **9** at $\lambda = 255$ nm (1 min, 20 mW). Negative bands are due to the consumption of **9** and the positive bands are due to the production of **a**-^{3}**10** (●, closed red circles) and **Z-11** (□, open blue squares). Further details regarding the identification of **a**-^{3}**10** and **Z-11** are discussed in the main text.

a-³10

Z-11
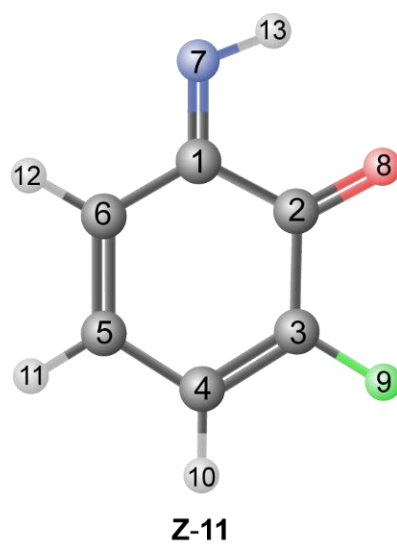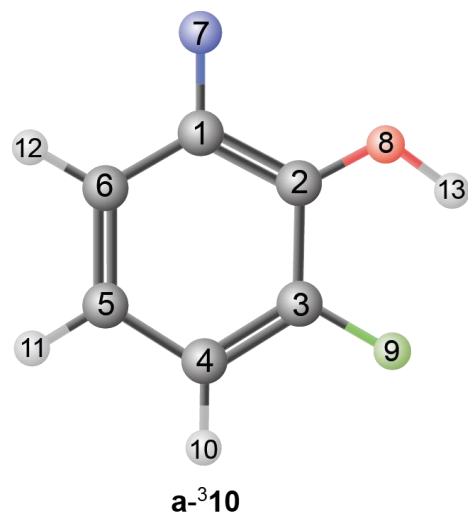
Figure S5. Geometry and atom numbering of triplet *anti*-3-fluoro-2-hydroxyphenylnitrene **a-³10** and (*Z*)-2-fluoro-6-iminocyclohexa-2,4-dienone **Z-11** used for the definition of internal coordinates. Color codes: blue – nitrogen, red – oxygen, green – fluor, gray – carbon, white – hydrogen.
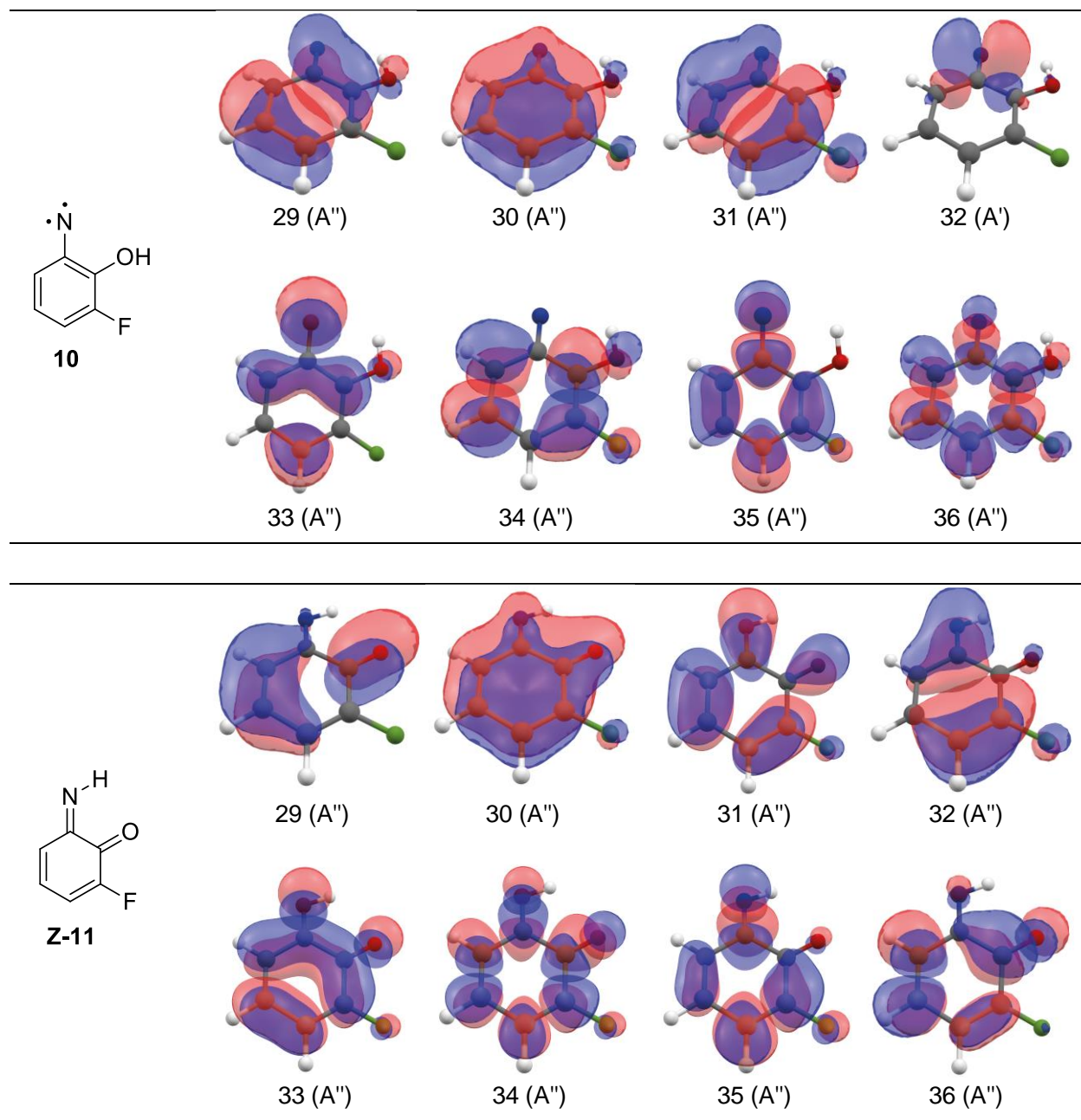
Figure S6. Active space orbitals used in the CASSCF(8,8) computations for nitrene **10** and imino **Z-11** species. Orbital occupation of each specific state can be found in *4 - Computational Section.*
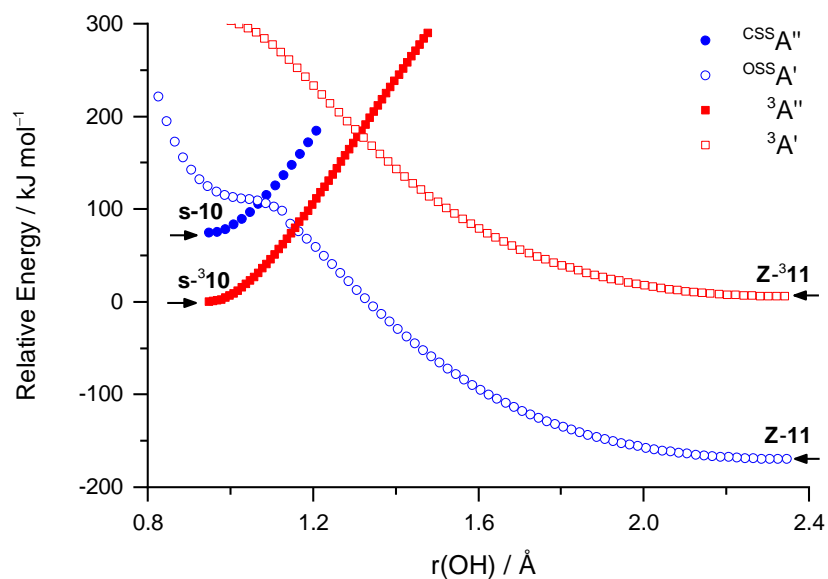
Figure S7. CASSCF(8,8)/6-31G(d) relaxed PES scans as a function of the OH distance for nitrene **10** and imino **Z-11**, considering the difference in the multiplicity [singlet (OSS and CSS) shown by blue circles and triplet by red squares] and symmetry [A' symmetry shown in open shape and A'' in closed shape]. The arrows indicate the starting point and direction of the scans.
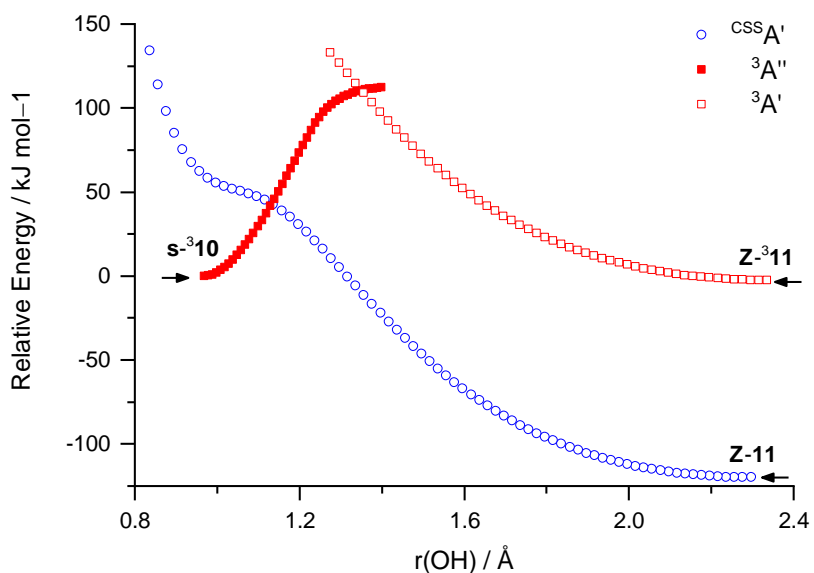
Figure S8. B3LYP/6-311+G(2d,p) relaxed PES scans as a function of the OH distance computed for nitrene **10** and imino **Z-11**, considering the difference in multiplicity [closed-shell singlet (CSS) shown in blue circles and triplet in red squares] and symmetry [A' symmetry shown in open shape and A'' in closed shape]. The arrows indicate the starting point and direction of the scans.
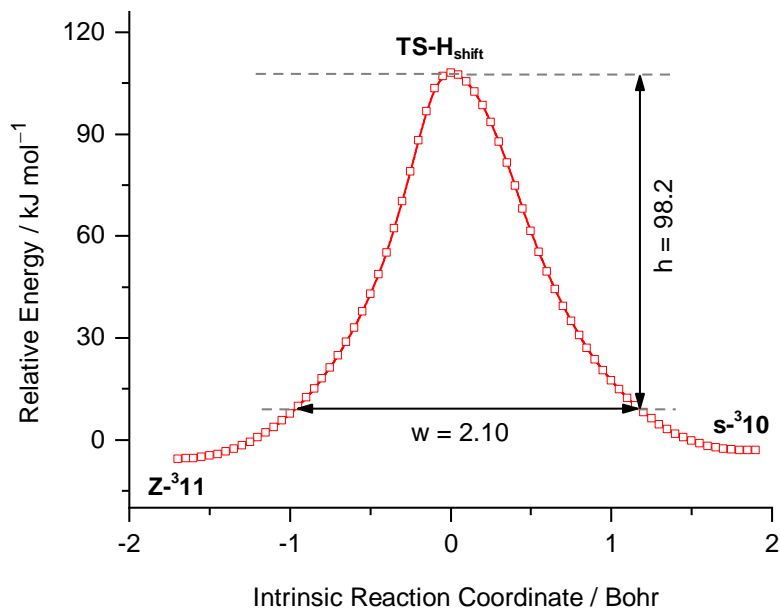
Figure S9. B3LYP/6-311+G(2d,p) intrinsic reaction coordinate (IRC) profile for the H-shift of **s-^{3}10** to **Z-^{3}11**. The relative electronic energy is given in relation to the energy of **s-^{3}10**. The vertical arrow establishes the zero-point corrected energy of the reactant **s-^{3}10** relative to the transition-state (h = 98.2 kJ mol^{-1}). The horizontal arrow establishes the barrier width considering the zero-point corrected energy values of the stationary points superimposed with the pure electronic IRC energy profile (w = 2.10 Bohr).
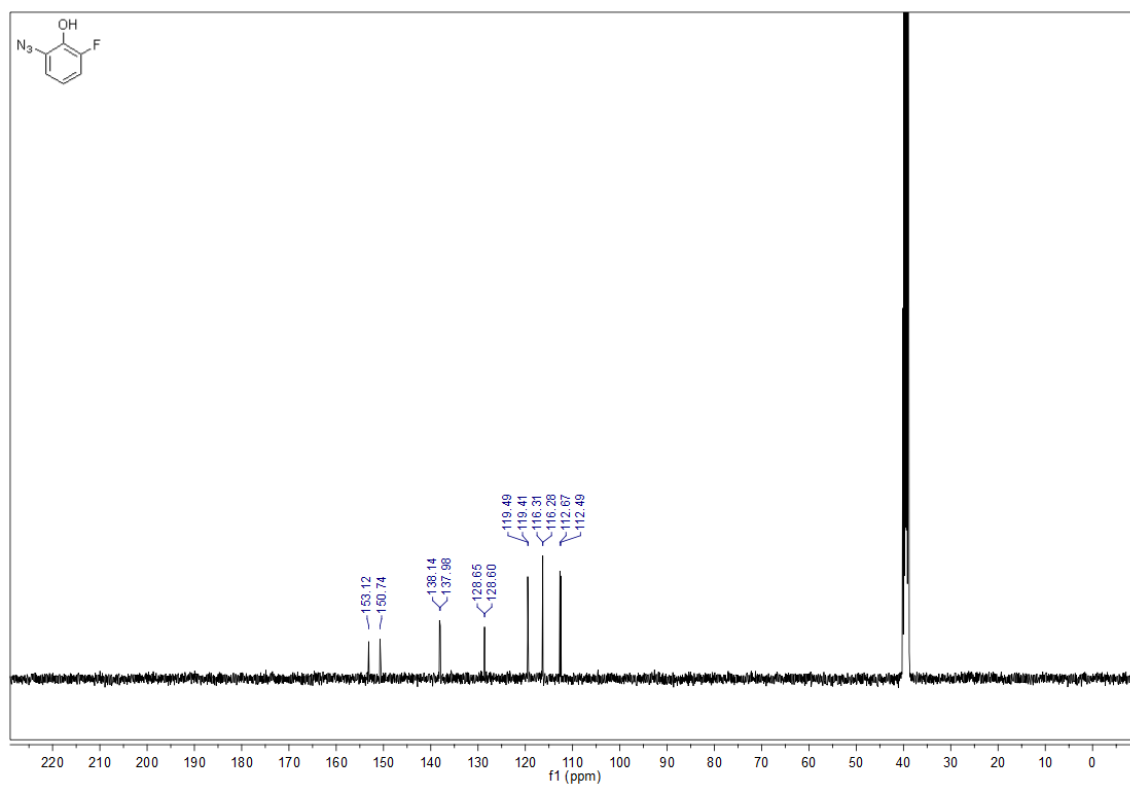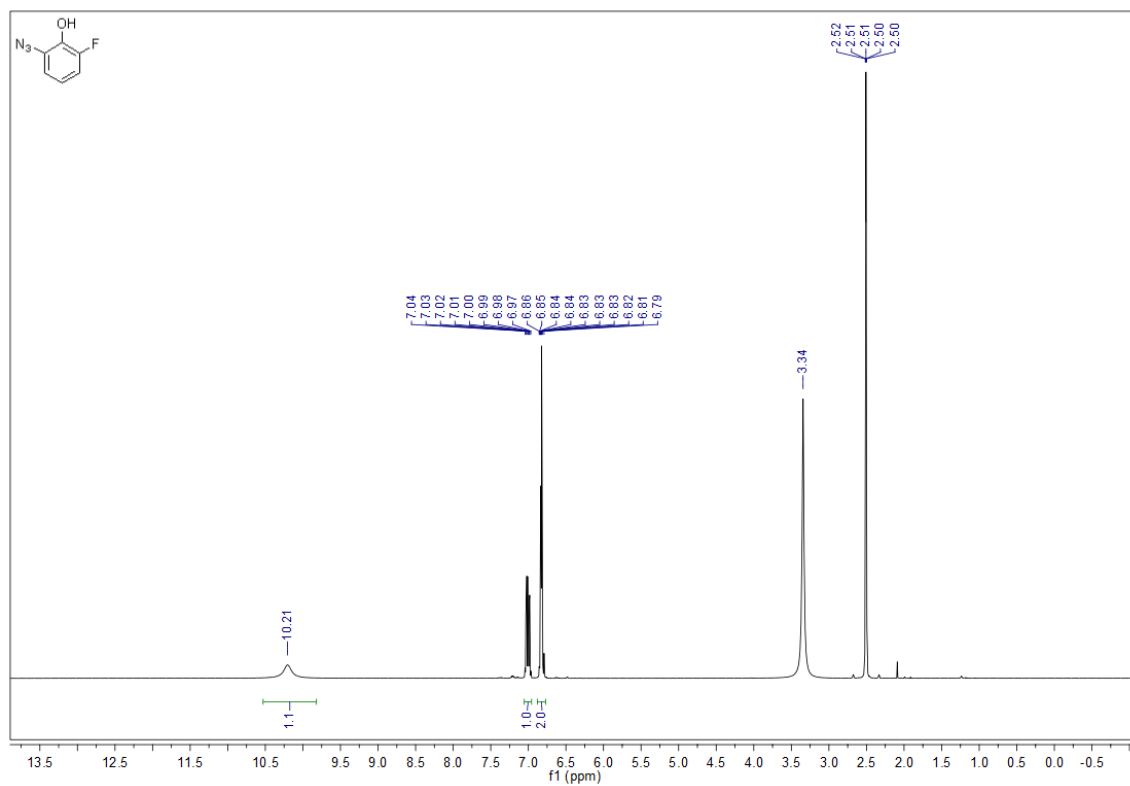
Figure S10. ^{1}H (top) and ^{13}C (bottom) NMR spectra of 3-fluoro-2-hydroxyphenylazide (**9**) in DMSO‑d$_6$.
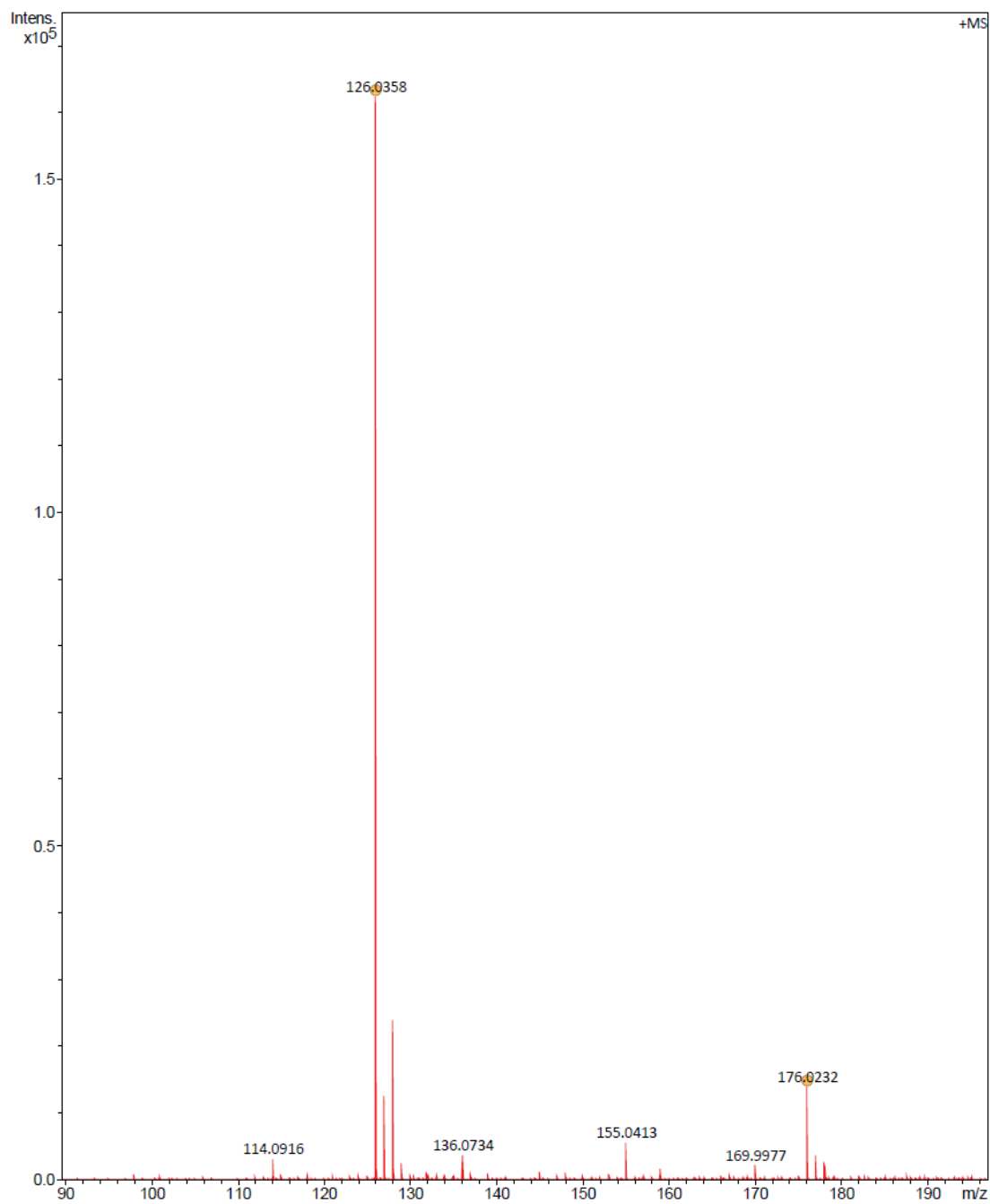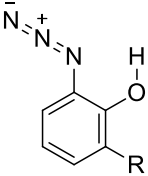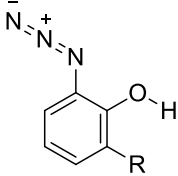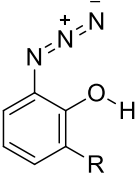
Figure S11. Electrospray ionization mass spectrum in positive-ion mode (HRMS-ESI$^+$) of 3-fluoro-2-hydroxyphenylazide (**9**).

3. Tables

Table S1. Relative Gibbs energy at 298 K (ΔG_{298K} in kJ mol^{-1}) computed at the B3LYP/6-311+G(2d,p) and CBS-QB3 levels of theory for conformers of 2-hydroxyphenylazide **9′** and 3-fluoro-2-hydroxyphenylazide **9** and their equilibrium populations at 298 K (Pop_{298K} in %).[a]

Structures **9′**, **9** R = H, F	as-9′ | as-9	aa-9′ | aa-9	sa-9′ | sa-9
Name	**as-9′** | as-9	**aa-9′** | aa-9	**sa-9′** | sa-9
ΔG_{298K} (B3LYP)	0.0 | 0.0	14.8 | 3.5	10.6 | 0.8
ΔG_{298K} (CBS-QB3)	0.0 | 0.0	15.5 | 4.5	12.8 | 2.6
Pop_{298K}	**99.2** | **66.1**	**0.2** | **10.7**	**0.6** | **23.1**

[a] Equilibrium populations were estimated from Boltzmann distribution based on the ΔG_{298K} value computed at the CBS-QB3 level of theory. In the names of structures, **a** stands for *anti* and **s** stands for *syn*, which corresponds to the orientation of the azido (first letter) and hydroxy (second letter) moieties, relative to one another.

Table S2. Definition of internal coordinates used in the normal mode analysis of a-^{3}**10**.[a]

Coordinate	Definition	Approximate description
S_1	$r_{8,13}$	$\nu(OH)$
S_2	$(3^{-1/2})(r_{6,12} + r_{5,11} + r_{4,10})$	$\nu_a(CH)$
S_3	$(2^{-1/2})(r_{6,12} - r_{4,10})$	$\nu_b(CH)$
S_4	$(6^{-1/2})(- r_{6,12} + 2r_{5,11} - r_{4,10})$	$\nu_c(CH)$
S_5	$(12^{-1/2})(2r_{3,4} - r_{4,5} - r_{5,6} + 2r_{6,1} - r_{1,2} - r_{2,3})$	$\nu_a(CC)$
S_6	$(4^{-1/2})(r_{4,5} - r_{5,6} + r_{1,2} - r_{2,3})$	$\nu_b(CC)$
S_7	$(4^{-1/2})(r_{4,5} + r_{5,6} - r_{1,2} - r_{2,3})$	$\nu_c(CC)$
S_8	$(12^{-1/2})(2r_{3,4} - r_{4,5} + r_{5,6} - 2r_{6,1} + r_{1,2} - r_{2,3})$	$\nu_d(CC)$
S_9	$(6^{-1/2})(r_{3,4} - r_{4,5} + r_{5,6} - r_{6,1} + r_{1,2} - r_{2,3})$	$\nu_e(CC)$
S_{10}	$(6^{-1/2})(r_{3,4} + r_{4,5} + r_{5,6} + r_{6,1} + r_{1,2} + r_{2,3})$	$\nu_f(CC)$
S_{11}	$r_{1,7}$	$\nu(C–N)$
S_{12}	$r_{2,8}$	$\nu(C–O)$
S_{13}	$r_{3,9}$	$\nu(C–F)$
S_{14}	$(6^{-1/2})(\beta_{1,12,6} - \beta_{5,12,6} + \beta_{6,11,5} - \beta_{4,11,5} + \beta_{5,10,4} - \beta_{3,10,4})$	$\delta_a(CH)$
S_{15}	$(4^{-1/2})(\beta_{1,12,6} - \beta_{5,12,6} - \beta_{5,10,4} + \beta_{3,10,4})$	$\delta_b(CH)$
S_{16}	$(12^{-1/2})(-\beta_{1,12,6} + \beta_{5,12,6} + 2\beta_{6,11,5} - 2\beta_{4,11,5} - \beta_{5,10,4} + \beta_{3,10,4})$	$\delta_c(CH)$
S_{17}	$(2^{-1/2})(\beta_{6,7,1} - \beta_{2,7,1})$	$\delta(C–N)$
S_{18}	$(2^{-1/2})(\beta_{4,9,3} - \beta_{2,9,3})$	$\delta(C–F)$
S_{19}	$(2^{-1/2})(\beta_{1,8,2} - \beta_{3,8,2})$	$\delta(C–O)$
S_{20}	$\beta_{2,13,8}$	$\delta(OH)$
S_{21}	$(6^{-1/2})(\beta_{3,1,2} - \beta_{2,6,1} + \beta_{1,5,6} - \beta_{6,4,5} + \beta_{5,3,4} - \beta_{4,2,3})$	$\delta_a(ring)$
S_{22}	$(12^{-1/2})(2\beta_{3,1,2} - \beta_{2,6,1} - \beta_{1,5,6} + 2\beta_{6,4,5} - \beta_{5,3,4} - \beta_{4,2,3})$	$\delta_b(ring)$
S_{23}	$(4^{-1/2})(\beta_{2,6,1} - \beta_{1,5,6} + \beta_{5,3,4} - \beta_{4,2,3})$	$\delta_c(ring)$
S_{24}	$(6^{-1/2})(\tau_{3,2,1,6} - \tau_{2,1,6,5} + \tau_{1,6,5,4} - \tau_{6,5,4,3} + \tau_{5,4,3,2} - \tau_{4,3,2,1})$	$\tau_a(ring)$
S_{25}	$(12^{-1/2})(-\tau_{32,1,6} + 2\tau_{2,1,6,5} - \tau_{1,6,5,4} - \tau_{6,5,4,3} + 2\tau_{5,4,3,2} - \tau_{4,3,2,1})$	$\tau_b(ring)$
S_{26}	$(4^{-1/2})(\tau_{3,2,1,6} - \tau_{1,6,5,4} + \tau_{6,5,4,3} - \tau_{4,3,2,1})$	$\tau_c(ring)$
S_{27}	$(2^{-1/2})(\tau_{13,8,2,1} - \tau_{13,8,2,3})$	$\tau(OH)$
S_{28}	$\gamma_{7,2,1,6}$	$\gamma(C-N)$
S_{29}	$\gamma_{8,3,2,1}$	$\gamma(C-O)$
S_{30}	$\gamma_{9,4,3,2}$	$\gamma(C-F)$
S_{31}	$(3^{-1/2})(\gamma_{12,1,6,5} + \gamma_{11,6,5,4} + \gamma_{10,5,4,3})$	$\gamma_a(CH)$
S_{32}	$(6^{-1/2})(- \gamma_{12,1,6,5} + 2\gamma_{11,6,5,4} - \gamma_{10,5,4,3})$	$\gamma_b(CH)$
S_{33}	$(2^{-1/2})(\gamma_{12,1,6,5} - \gamma_{10,5,4,3})$	$\gamma_c(CH)$

[a] Abbreviations: ν = stretching, δ = in-plane bending, γ = out-of-plane bending, τ = torsion, ring = 6-member ring (benzene). See Figure S5 for the atom numbering scheme; $r_{i,j}$ is the distance between atoms A_i and A_j; $\beta_{i,j,k}$ is the angle between vectors A_kA_i and A_kA_j; $\tau_{i,j,k,l}$ is the dihedral angle between the plane defined by A_i, A_j, A_k and the plane defined by A_j, A_k and A_l atoms; $\gamma_{i,j,k,l}$ is the angle between the vector A_kA_i and the plane defined by atoms A_j, A_k, A_l. The combinations [(+), (+)] and [(+), (−)] denote in-phase and in-opposite-phase couplings between coordinates of different types.

Table S3. Definition of internal coordinates used in the normal mode analysis of **Z-11**.[a]

Coordinate	Definition	Approximate description
S_1	$r_{7,13}$	$\nu(NH)$
S_2	$(3^{-1/2})(r_{6,12} + r_{5,11} + r_{4,10})$	$\nu_a(CH)$
S_3	$(2^{-1/2})(r_{6,12} - r_{4,10})$	$\nu_b(CH)$
S_4	$(6^{-1/2})(-r_{6,12} + 2r_{5,11} - r_{4,10})$	$\nu_c(CH)$
S_5	$r_{2,8}$	$\nu(C=O)$
S_6	$r_{1,7}$	$\nu(C=N)$
S_7	$(2^{-1/2})(r_{4,3} - r_{6,5})$	$\nu(C=C)_{as}$
S_8	$(2^{-1/2})(r_{4,3} + r_{6,5})$	$\nu(C=C)_{s}$
S_9	$(2^{-1/2})(r_{2,3} - r_{4,5})$	$\nu_a(C-C)_{as}$
S_{10}	$(2^{-1/2})(r_{2,3} + r_{4,5})$	$\nu_a(C-C)_{s}$
S_{11}	$(2^{-1/2})(r_{2,1} - r_{1,6})$	$\nu_b(C-C)_{as}$
S_{12}	$(2^{-1/2})(r_{2,1} + r_{1,6})$	$\nu_b(C-C)_{s}$
S_{13}	$r_{3,9}$	$\nu(C-F)$
S_{14}	$(6^{-1/2})(\beta_{1,12,6} - \beta_{5,12,6} + \beta_{6,11,5} - \beta_{4,11,5} + \beta_{5,10,4} - \beta_{3,10,4})$	$\delta_a(CH)$
S_{15}	$(4^{-1/2})(\beta_{1,12,6} - \beta_{5,12,6} - \beta_{5,10,4} + \beta_{3,10,4})$	$\delta_b(CH)$
S_{16}	$(12^{-1/2})(-\beta_{1,12,6} + \beta_{5,12,6} + 2\beta_{6,11,5} - 2\beta_{4,11,5} - \beta_{5,10,4} + \beta_{3,10,4})$	$\delta_c(CH)$
S_{17}	$(2^{-1/2})(\beta_{6,7,1} - \beta_{2,7,1})$	$\delta(C=N)$
S_{18}	$(2^{-1/2})(\beta_{4,9,3} - \beta_{2,9,3})$	$\delta(C-F)$
S_{19}	$(2^{-1/2})(\beta_{1,8,2} - \beta_{3,8,2})$	$\delta(C=O)$
S_{20}	$\beta_{1,13,7}$	$\delta(NH)$
S_{21}	$(6^{-1/2})(\beta_{3,1,2} - \beta_{2,6,1} + \beta_{1,5,6} - \beta_{6,4,5} + \beta_{5,3,4} - \beta_{4,2,3})$	$\delta_a(ring)$
S_{22}	$(12^{-1/2})(2\beta_{3,1,2} - \beta_{2,6,1} - \beta_{1,5,6} + 2\beta_{6,4,5} - \beta_{5,3,4} - \beta_{4,2,3})$	$\delta_b(ring)$
S_{23}	$(4^{-1/2})(\beta_{2,6,1} - \beta_{1,5,6} + \beta_{5,3,4} - \beta_{4,2,3})$	$\delta_c(ring)$
S_{24}	$(6^{-1/2})(\tau_{3,2,1,6} - \tau_{2,1,6,5} + \tau_{1,6,5,4} - \tau_{6,5,4,3} + \tau_{5,4,3,2} - \tau_{4,3,2,1})$	$\tau_a(ring)$
S_{25}	$(12^{-1/2})(-\tau_{32,1,6} + 2\tau_{2,1,6,5} - \tau_{1,6,5,4} - \tau_{6,5,4,3} + 2\tau_{5,4,3,2} - \tau_{4,3,2,1})$	$\tau_b(ring)$
S_{26}	$(4^{-1/2})(\tau_{3,2,1,6} - \tau_{1,6,5,4} + \tau_{6,5,4,3} - \tau_{4,3,2,1})$	$\tau_c(ring)$
S_{27}	$(2^{-1/2})(\tau_{13,7,1,2} - \tau_{13,7,1,6})$	$\tau(NH)$
S_{28}	$\gamma_{7,2,1,6}$	$\gamma(C=N)$
S_{29}	$\gamma_{8,3,2,1}$	$\gamma(C=O)$
S_{30}	$\gamma_{9,4,3,2}$	$\gamma(C-F)$
S_{31}	$(3^{-1/2})(\gamma_{12,1,6,5} + \gamma_{11,6,5,4} + \gamma_{10,5,4,3})$	$\gamma_a(CH)$
S_{32}	$(6^{-1/2})(-\gamma_{12,1,6,5} + 2\gamma_{11,6,5,4} - \gamma_{10,5,4,3})$	$\gamma_b(CH)$
S_{33}	$(2^{-1/2})(\gamma_{12,1,6,5} - \gamma_{10,5,4,3})$	$\gamma_c(CH)$

[a] Abbreviations: ν = stretching, δ = in-plane bending, γ = out-of-plane bending, τ = torsion, ring = six-membered ring. See Figure S5 for the atom numbering scheme; $r_{i,j}$ is the distance between atoms A_i and A_j; $\beta_{i,j,k}$ is the angle between vectors A_kA_i and A_kA_j; $\tau_{i,j,k,l}$ is the dihedral angle between the plane defined by A_i, A_j, A_k and the plane defined by A_j, A_k and A_l atoms; $\gamma_{i,j,k,l}$ is the angle between the vector A_kA_i and the plane defined by atoms A_j, A_k, A_l. The combinations [(+), (+)] and [(+), (−)] denote in-phase and in-opposite-phase couplings between coordinates of different types.

Table S4. Experimental IR spectral data (nitrogen matrix at 10 K), B3LYP/6-311+G(2d,p) computed vibrational frequencies ($\tilde{v}$, cm^{-1}) and infrared intensities (A^{th}, km mol^{-1}), and vibrational assignment of triplet *anti*-3-fluoro-2-hydroxyphenylnitrene **a-^{3}10**.

Experimental[a]		Computed[b]		PED[c]
$\tilde{v}$	I	$\tilde{v}$	A^{th}	
3576	br	3596	130.2	100.0[ν(OH)]
1571	s	1564	55.8	35.2[ν_b(CC)] ; 29.4[ν_a(CC)]
1538	s	1536	75.9	21.8[ν_b(CC)] ; 20.1[ν_a(CC)] : 17.2[δ_b(CH)]
1444	vs	1433	141.8	26.0[δ_a(CH)] ; 17.6[ν(C−O)] ; 12.3[ν_e(CC)] ; 10.1[ν_a(CC)]
		1420	8.4	20.9[ν_c(CC)] ; 20.9[δ_b(CH)] ; 17.4[δ_a(CH)] 14.6[δ(OH)]
1339	m	1344	37.2	40.5[ν_e(CC)] + 34.4[δ(OH)]
1303	w	1298	26.5	50.7[ν(C−N)] ; 16.7[δ_a(ring)] ; 10.2[ν(C−O)]
1249	w	1244	79.5	29.7[δ_a(CH)] ; 12.6[ν_d(CC)] ; 12.6[ν_f(CC)] ; 12.2[ν(C−F)]
1230	m	1220	64.7	53.6[ν_e(CC)] − 26.1[δ(OH)]
1191/1187	w	1175	24.3	18.3[ν(C−O)] ; 16.6[ν_d(CC)] ; 16.3[ν(C−F)] ; 14.1[ν_a(CC)] ; 11.4[ν(C−N)]
1144	w	1139	20.8	59.9[δ_c(CH)] ; 18.9[ν_b(CC)]
1056	w	1051	15.0	35.6[ν_c(CC)] ; 29.4[δ_b(CH)] ; 16.6[ν_f(CC)]
996/990	s	978	103.1	25.2[ν(C−F)] ; 24.0[ν_d(CC)]
		938	0.2	116.0[γ_b(CH)]
		851	0.1	99.5[γ_c(CH)]
		823	7.8	49.8[δ_a(ring)] ; 15.7[ν(C−O)] ; 12.3[δ_b(ring)]
768/765	m	754	47.1	67.5[γ_a(CH)] ; 13.9[γ(C-N)] 11.5[γ(C-F)]
696	w	686	17.6	52.6[ν_f(CC)] ; 13.1[ν(C−F)]
693	w	681	21.7	30.4[τ_a(ring)] ; 30.1[γ_a(CH)] ; 29.6[γ(C-O)] ; 13.2[γ(C-N)]

[a] Experimental intensities (I) are given in qualitative terms: vs = very strong s = strong; m = medium; w = weak; br = broad. The IR spectrum reported corresponds to the region between 1750 and 600 cm^{-1} and the ν(OH) mode. [b] Computed harmonic wavenumbers (cm^{-1}) were multiplied by a 0.979 factor, except the ν(OH) mode which multiplied by a 0.950 factor. [c] Abbreviations: ν = stretching, δ = in-plane bending, γ = out-of-plane bending, τ = torsion, ring = six-membered ring (benzene). PEDs are expressed in %, and the PED matrices lower than 10% are not included. Definition of internal coordinates is given in Table S2.

Table S5. Experimental IR spectral data (nitrogen matrix at 10 K), B3LYP/6-311+G(2d,p) computed vibrational frequencies ($\tilde{v}$, cm^{-1}) and infrared intensities (A^{th}, km mol^{-1}), and vibrational assignment of (Z)-2-fluoro-6-iminocyclohexa-2,4-dienone **Z-11**.

Experimental[a]		Calculated[b]		PED[c]
$\tilde{v}$	I	$\tilde{v}$	A^{th}	
3216	br	3218	14	99.9 [ν(NH)]
1691	s	1701	170.3	81.3[ν(C=O)]
1648	s	1659	53.3	62.5[ν(C=C)$_{as}$] ; 10.2[δ$_b$(CH)]
		1604	38.9	75.5[ν(C=N)]
1576	w	1576	8.9	69.3[ν(C=C)$_s$]
1417/1407	w	1410	5.9	21.0[δ$_a$(CH)] ; 14.8[ν$_b$(C–C)$_{as}$] ; 14.4[δ$_b$(CH)] ; 12.9[δ$_c$(CH)] ; 11.7[δ(NH)]
1358	m	1347	30.0	46.9[δ(NH)] ; 20.8[δ$_b$(CH)]
1347	m	1340	61.7	39.5[δ$_a$(CH)] ; 13.2[ν$_a$(C–C)$_{as}$] ; 11.9[ν$_a$(C–C)$_s$]
1256	m	1241	67.8	34.3[ν(C–F)] ; 16.3[δ$_b$(CH)] ; 15.2[δ$_a$(CH)] ; 13.7[ν$_a$(C–C)$_s$]
1164	m	1163	40.9	57.2[δ$_c$(CH)]
1114	s	1098	104.9	37.7[ν$_b$(C–C)$_{as}$] ; 18.8[δ(NH)] ; 15.5[δ$_c$(CH)]
1018	w	1012	20.2	31.0[ν$_a$(C–C)$_{as}$] 14.5[δ$_b$(CH)]
993	s	979	35.5	21.7[ν$_a$(C–C)$_s$] ; 19.5[δ(C=O)] ; 18.2[ν$_b$(C–C)$_s$] 13.1[ν(C–F)]
		978	2.1	92.1[γ$_b$(CH)] ; 14.0[γ$_c$(CH)] ; 10.5[τ(NH)]
937	w	953	28.0	78.8[τ(NH)] ; 16.7[γ$_b$(CH)]
		911	4.9	81.2[γ$_c$(CH)] ; 12.2[γ$_a$(CH)]
836	m	828	34.4	64.2[δ$_a$(ring]
		823	3.8	29.3[γ$_a$(CH)] ; 27.9[γ(C=O)] ; 26.9[γ(C=N)] ; 9.7[γ(C-F)]
727	m	723	88.4	52.9[γ$_a$(CH)] ; 19.8[γ(C=O)] ; 17.2[τ$_a$(ring)]
		670	3.9	29.9[ν$_b$(C–C)$_s$] ; 21.8[ν$_a$(C–C)$_s$] ; 11.5[ν(C=C)$_s$]

[a] Experimental intensities (I) are given in qualitative terms: s = strong; m = medium; w = weak; br = broad. The IR spectrum reported corresponds to the region between 1750 and 600 cm^{-1} and the ν(NH) mode. [b] Computed harmonic wavenumbers (cm^{-1}) were multiplied by a 0.979 factor, except for the ν(NH) mode which multiplied by a 0.950 factor. [c] Abbreviations: ν = stretching, δ = in-plane bending, γ = out-of-plane bending, τ = torsion, ring = six-membered ring. PEDs are expressed in %, and the PED matrices lower than 10% are not included. Definition of internal coordinates is given in Table S3.

4. Computational Section

Optimized geometries (Cartesian coordinates, Å), electronic energies (E, E_h) and zero-point vibrational energy (ZPVE, E_h) computed at the B3LYP/6-311+G(2d,p), CBS-QB3 and CASSCF(8,8)/6-31G(d) levels of theory.

as-9'

B3LYP (E = -471.205545; ZPVE = 0.107459)   CBS-QB3 (E = -470.325318; ZPVE = 0.106642)

C	0.876096	0.944931	0.000006	-0.872245	0.950633	0.000002
C	-0.199146	0.044211	0.000032	0.198145	0.038782	-0.000001
C	0.035767	-1.328335	0.000032	-0.044497	-1.334432	0.000001
C	1.339474	-1.808128	0.000002	-1.353364	-1.806896	0.000006
C	2.406391	-0.913722	-0.000024	-2.415937	-0.903870	0.000009
C	2.177104	0.456687	-0.000022	-2.178427	0.467356	0.000007
O	0.672545	2.288987	0.000008	-0.656072	2.290106	0.000001
H	-0.281055	2.456711	0.000023	0.299780	2.438893	-0.000003
N	-1.483298	0.656112	0.000069	1.484145	0.648824	-0.000006
N	-2.485112	-0.058578	-0.000016	2.487523	-0.063434	-0.000009
N	-3.467545	-0.616059	-0.000082	3.474800	-0.619983	-0.000011
H	-0.799461	-2.019441	0.000055	0.788236	-2.029457	-0.000002
H	1.518499	-2.875673	0.000002	-1.539291	-2.873874	0.000007
H	3.424187	-1.283691	-0.000046	-3.436758	-1.267377	0.000013
H	2.995041	1.166002	-0.000043	-2.990717	1.183686	0.000010

aa-9'

B3LYP (E = -471.199342; ZPVE = 0.107022)   CBS-QB3 (E = -470.319212; ZPVE = 0.106292)

C	0.899628	0.921892	0.000007	-0.898903	0.926762	0.000000
C	-0.220214	0.075129	-0.000010	0.220847	0.073494	0.000000
C	-0.033114	-1.306463	-0.000008	0.029305	-1.309353	0.000000
C	1.245460	-1.850789	-0.000002	-1.252839	-1.851842	0.000000
C	2.352087	-1.010718	-0.000001	-2.358471	-1.007591	0.000000
C	2.175582	0.368733	0.000014	-2.177963	0.374007	0.000000
O	0.676141	2.266451	-0.000014	-0.668384	2.267754	0.000000
H	1.520616	2.731262	-0.000004	-1.512515	2.730650	0.000000
N	-1.487416	0.707021	0.000008	1.489050	0.704134	0.000000
N	-2.494134	0.000847	0.000008	2.495506	-0.002960	0.000000
N	-3.491413	-0.532165	0.000000	3.497656	-0.534654	0.000000
H	-0.897547	-1.960434	-0.000012	0.893532	-1.964603	0.000000
H	1.371603	-2.925905	-0.000008	-1.381270	-2.927304	0.000000
H	3.353492	-1.422543	0.000004	-3.361784	-1.416412	0.000000
H	3.036877	1.029381	0.000024	-3.038234	1.037130	0.000000

sa-9'

B3LYP (*E* = -471.199578; ZPVE = 0.106834)   CBS-QB3 (*E* = -470.319660; ZPVE = 0.106031)

C	0.260703	0.820334	-0.000003	-0.256950	0.821906	0.000001
C	-0.027894	-0.553835	-0.000005	0.027017	-0.557375	0.000000
C	1.031836	-1.461959	-0.000002	-1.037015	-1.463244	-0.000001
C	2.349569	-1.027861	0.000004	-2.355851	-1.024137	-0.000002
C	2.627538	0.334417	0.000007	-2.629743	0.340827	-0.000001
C	1.582528	1.250801	0.000003	-1.580195	1.256134	0.000000
O	-0.797272	1.688065	-0.000009	0.806273	1.679946	0.000002
H	-0.476549	2.596750	-0.000001	0.489432	2.588616	0.000003
N	-1.320112	-1.118918	-0.000012	1.319040	-1.122492	0.000000
N	-2.352830	-0.443208	0.000003	2.350422	-0.444597	0.000002
N	-3.395304	-0.010403	0.000015	3.395414	-0.008407	-0.000002
H	0.792748	-2.517861	-0.000004	-0.797915	-2.519557	-0.000002
H	3.154271	-1.751900	0.000006	-3.163208	-1.746153	-0.000003
H	3.650878	0.688059	0.000012	-3.652501	0.698037	-0.000001
H	1.788865	2.316746	0.000004	-1.783701	2.323281	0.000001

as-9

B3LYP (*E* = -570.470642; ZPVE = 0.099307)   CBS-QB3 (*E* = -569.487174; ZPVE = 0.098506)

C	-0.651871	-0.729403	0.000000	0.650089	-0.730728	0.000001
C	0.536322	0.014850	0.000006	-0.535992	0.021342	-0.000002
C	0.507597	1.408121	0.000004	-0.503397	1.417256	0.000000
C	-0.711976	2.071246	-0.000003	0.720691	2.075841	0.000005
C	-1.902879	1.350965	-0.000009	1.909882	1.347518	0.000008
C	-1.855172	-0.030087	-0.000007	1.859961	-0.035703	0.000006
O	-0.664322	-2.083115	0.000002	0.653687	-2.083220	0.000000
H	0.252699	-2.394651	0.000008	-0.267411	-2.379142	-0.000004
N	1.712276	-0.781975	0.000011	-1.712540	-0.776172	-0.000008
N	2.809740	-0.222951	0.000008	-2.812256	-0.222284	-0.000010
N	3.863963	0.180351	0.000004	-3.872081	0.177125	-0.000012
H	1.434340	1.969106	0.000008	-1.429628	1.980130	-0.000003
H	-0.736670	3.152991	-0.000005	0.751140	3.157983	0.000006
H	-2.867140	1.841886	-0.000015	2.877590	1.832658	0.000012
F	-3.000292	-0.738503	-0.000013	3.001060	-0.749968	0.000010

aa-9

B3LYP (*E* = -570.469178; ZPVE = 0.099174)   CBS-QB3 (*E* = -569.529129; ZPVE = 0.098414)

C	0.660174	-0.718145	0.000000	0.660198	-0.719481	0.000000
C	-0.559333	-0.027028	0.000002	-0.560703	-0.025767	0.000000
C	-0.561099	1.369645	0.000002	-0.560731	1.373717	0.000000
C	0.631294	2.081276	0.000000	0.633761	2.085822	0.000000
C	1.850353	1.410504	0.000000	1.853932	1.411991	0.000000
C	1.830196	0.031745	0.000001	1.833789	0.031027	0.000000
O	0.674044	-2.073894	0.000000	0.674182	-2.074247	0.000000
H	1.592456	-2.374724	0.000002	1.594874	-2.364212	0.000000
N	-1.722968	-0.829382	0.000004	-1.724509	-0.828413	0.000001
N	-2.818985	-0.268991	-0.000001	-2.821159	-0.268921	0.000000
N	-3.880423	0.118154	-0.000005	-3.887840	0.114813	-0.000001
H	-1.505123	1.900912	0.000004	-1.505739	1.904421	0.000000
H	0.611659	3.163129	-0.000002	0.614975	3.168234	0.000000
H	2.797567	1.933034	-0.000001	2.803213	1.931632	-0.000001
F	2.995356	-0.673072	-0.000003	2.996923	-0.679147	0.000000

sa-9

B3LYP (*E* = -570.469343; ZPVE = 0.099036)   CBS-QB3 (*E* = -569.529865; ZPVE = 0.098204)

C	-0.173711	-0.521867	-0.000001	-0.170769	-0.521289	0.000000
C	0.388485	0.762175	-0.000006	0.388123	0.767052	0.000001
C	-0.459980	1.873008	0.000001	-0.465574	1.877318	0.000002
C	-1.838240	1.722496	0.000003	-1.845452	1.722015	0.000001
C	-2.408325	0.451832	-0.000001	-2.411687	0.446886	0.000000
C	-1.558671	-0.632819	0.000000	-1.558393	-0.637872	0.000000
O	0.632427	-1.618747	0.000005	0.639356	-1.614449	0.000000
H	0.083471	-2.413953	-0.000005	0.087005	-2.405785	-0.000003
N	1.769248	1.038169	-0.000001	1.768613	1.043642	0.000002
N	2.628585	0.149709	0.000000	2.625597	0.152929	-0.000001
N	3.548906	-0.502162	0.000001	3.547183	-0.503476	-0.000002
H	-0.007358	2.855785	0.000003	-0.012770	2.860444	0.000003
H	-2.474921	2.597373	0.000006	-2.485622	2.595041	0.000002
H	-3.478795	0.296168	0.000000	-3.481743	0.285599	0.000000
F	-2.056260	-1.901595	-0.000001	-2.047662	-1.910671	-0.000001

a-³10

B3LYP (*E* = -460.906470; ZPVE = 0.087242)   CASSCF(8,8) (*E* = -458.294809; ZPVE = 0.092045)

Orbital occupation: **29** - 1.95; **30** - 1.89; **31** - 1.89; **32** - 1.00;
33 - 1.00; **34** - 0.11; **35** - 0.12; **36** - 0.04

C	-0.169030	-0.742130	0.000000	0.000000	0.759581	0.000000
C	1.238506	-0.458095	-0.000001	1.294995	0.170564	0.000000
C	1.644889	0.917825	0.000000	1.398225	-1.252334	0.000000
C	0.716908	1.931897	0.000000	0.264378	-2.046989	0.000000
C	-0.656394	1.643440	0.000000	-1.011878	-1.459829	0.000000
C	-1.055344	0.320885	0.000000	-1.104372	-0.074421	0.000000
O	-0.576821	-2.027133	0.000000	-0.108218	2.100257	0.000000
H	-1.543810	-2.052492	0.000000	-1.023261	2.350722	0.000000
N	2.131575	-1.427827	0.000000	2.398981	0.928436	0.000000
H	2.706529	1.125413	0.000000	2.379580	-1.687916	0.000000
H	1.042872	2.964029	0.000000	0.356416	-3.116776	0.000000
H	-1.405271	2.424316	0.000000	-1.909574	-2.047609	0.000000
F	-2.380443	0.007518	0.000000	-2.308707	0.513448	0.000000

s-³10

B3LYP (*E* = -460.907658; ZPVE = 0.087321)   CASSCF(8,8) (*E* = -458.293127; ZPVE = 0.091971)

Orbital occupation: **29** - 1.89; **30** - 1.95; **31** - 1.89; **32** - 1.00;
33 - 1.00; **34** - 0.11; **35 -** 0.11; **36** - 0.04

C	-0.055429	-0.758352	0.000000	-2.023770	1.248816	0.083925
C	1.281564	-0.222297	0.000000	-2.258265	0.555554	1.306119
C	1.453497	1.201343	0.000000	-2.728437	-0.792268	1.267415
C	0.358494	2.028438	0.000000	-2.952792	-1.415352	0.055546
C	-0.941994	1.496619	0.000000	-2.719815	-0.726584	-1.149517
C	-1.123387	0.125100	0.000000	-2.262661	0.584014	-1.110542
O	-0.283584	-2.085212	0.000000	-1.581113	2.519317	0.045204
H	0.565656	-2.551163	0.000000	-1.456710	2.861398	0.920615
N	2.296283	-1.058997	0.000000	-2.035153	1.175649	2.468399
H	2.462380	1.591107	0.000000	-2.899708	-1.299414	2.198092
H	0.491751	3.102657	0.000000	-3.306277	-2.428899	0.027616
H	-1.814574	2.136626	0.000000	-2.886454	-1.188326	-2.103738
F	-2.371888	-0.378851	0.000000	-2.044830	1.228435	-2.250261

a-^{OSS}10

CASSCF(8,8) (*E* = -458.265910; ZPVE = 0.091230)

Orbital occupation: **29** - 1.94; **30** - 1.91; **31** - 1.89; **32** - 1.00; **33** - 1.00; **34** - 0.10; **35** - 0.11; **36** - 0.05

C	-0.225262	0.741431	0.000009
C	1.230674	0.527714	-0.000001
C	1.700209	-0.870447	0.000007
C	0.813642	-1.908819	-0.000003
C	-0.594720	-1.675665	-0.000005
C	-1.052297	-0.343743	0.000003
O	-0.658156	2.012529	0.000006
H	-1.607289	2.030892	0.000000
N	2.053491	1.502238	-0.000019
H	2.760651	-1.032758	0.000011
H	1.172625	-2.921137	0.000001
H	-1.305158	-2.478040	-0.000007
F	-2.373721	-0.115297	0.000002

s-^{OSS}10

CASSCF(8,8) (*E* = -458.264936; ZPVE = 0.090940)

Orbital occupation: **29** - 1.89; **30** - 1.94; **31** - 1.91; **32** - 1.00; **33** - 1.00; **34** - 0.09; **35** - 0.11; **36 -** 0.05

C	-2.017179	1.268339	0.056366
C	-2.252901	0.570573	1.332106
C	-2.737267	-0.817931	1.275932
C	-2.954616	-1.420909	0.071706
C	-2.719695	-0.726132	-1.153011
C	-2.255879	0.603649	-1.113984
O	-1.574821	2.537277	0.049019
H	-1.458456	2.855870	0.934913
N	-2.036743	1.171973	2.436872
H	-2.907713	-1.322696	2.207002
H	-3.308171	-2.434455	0.034914
H	-2.887056	-1.189956	-2.104701
F	-2.045490	1.226738	-2.268262

a-^{CSS}10

CASSCF(8,8) (E = -458.228879; ZPVE = 0.093165)

Orbital occupation: **29** - 1.90; **30** - 1.96; **31** - 1.91; **32 -** 1.62; **33** - 0.40; **34** - 0.03; **35** - 0.08; **36** - 0.09

C	-0.130632	0.751156	-0.000003
C	1.242914	0.409400	0.000015
C	1.599289	-0.967194	-0.000017
C	0.640251	-1.964749	-0.000006
C	-0.719281	-1.613022	0.000002
C	-1.071128	-0.280218	-0.000004
O	-0.512148	2.028759	-0.000023
H	-1.459474	2.085920	-0.000032
N	2.197094	1.364490	0.000039
H	2.646880	-1.201081	-0.000036
H	0.922972	-3.000303	-0.000012
H	-1.495140	-2.355617	0.000012
F	-2.362910	0.075260	0.000008

TS-OH_{rot}

B3LYP (E = -460.897541; ZPVE = 0.085957)

C	0.128349	-0.753984	0.007462
C	-1.255103	-0.364306	0.002683
C	-1.575211	1.032461	-0.002343
C	-0.574532	1.977152	-0.003988
C	0.770717	1.592148	-0.004227
C	1.089744	0.239395	0.002361
O	0.472770	-2.071934	0.107190
H	0.611667	-2.467635	-0.762091
N	-2.215902	-1.269358	-0.007977
H	-2.619685	1.314171	-0.003358
H	-0.825803	3.030352	-0.005880
H	1.571711	2.319718	-0.007814
F	2.387498	-0.119203	-0.003802

Z-³11

B3LYP (*E* = -460.908591; ZPVE = 0.086885)   CASSCF(8,8) (*E* = -458.290950; ZPVE = 0.091681)

Orbital occupation: **29** - 1.94; **30** - 1.91; **31** - 1.03; **32** - 1.88;

33 - 0.97; **34** - 0.10; **35** - 0.12; **36** - 0.05

C	-0.076310	-0.839142	-0.000006	-0.028622	-0.831968	-0.055221
C	-1.304504	0.000546	0.000000	1.298462	-0.159732	-0.028015
C	-1.161148	1.394963	0.000000	1.342238	1.237190	0.015609
C	0.118120	2.029329	0.000000	0.136402	2.040726	0.035119
C	1.269461	1.290108	0.000001	-1.096202	1.446205	0.010729
C	1.166740	-0.119670	-0.000002	-1.174506	0.027287	-0.034101
O	-0.128483	-2.080594	0.000003	-0.128065	-2.057766	-0.093291
H	-2.406085	-1.563292	-0.000002	2.205023	-1.848094	-0.076559
N	-2.516086	-0.542967	0.000001	2.427940	-0.865764	-0.044745
H	-2.063817	1.993542	0.000001	2.304710	1.710929	0.034383
H	0.170507	3.110609	0.000001	0.222920	3.109906	0.069181
H	2.251794	1.744115	0.000003	-2.009102	2.010171	0.024246
F	2.290434	-0.819584	0.000001	-2.365191	-0.532218	-0.057329

Z-11

B3LYP (*E* = -460.953305; ZPVE = 0.089351)   CASSCF(8,8) (*E* = -458.356915; ZPVE = 0.094747)

Orbital occupation: **29** - 1.92; **30** - 1.94; **31 -** 1.85; **32** - 1.9;

33 - 0.17; **34** - 0.05; **35** - 0.09; **36** - 0.08

C	-0.046141	-0.854440	-0.000004	-0.039481	-0.843419	-0.000146
C	1.320381	-0.152972	-0.000002	1.311954	-0.168488	-0.000033
C	1.356654	1.305579	-0.000001	1.351273	1.298539	-0.000004
C	0.215125	2.013844	0.000000	0.212530	2.023581	-0.000003
C	-1.091474	1.374276	0.000002	-1.108158	1.384223	-0.000013
C	-1.212893	0.038017	0.000000	-1.214840	0.045911	-0.000046
O	-0.129200	-2.064857	-0.000001	-0.140246	-2.048775	0.000188
H	2.156313	-1.839169	0.000008	2.185982	-1.836474	-0.000042
N	2.395264	-0.839753	0.000004	2.395416	-0.850218	0.000020
H	2.331017	1.776602	-0.000004	2.321543	1.757095	0.000029
H	0.241249	3.096408	-0.000003	0.248109	3.096776	0.000034
H	-1.986353	1.985322	0.000005	-1.996716	1.986834	0.000031
F	-2.413932	-0.551985	0.000001	-2.391356	-0.558713	-0.000010

TS-H_{shift}

B3LYP (E = -460.865278; ZPVE = 0.082345)

C	0.154803	-0.728945	-0.016784
C	1.248903	0.211022	0.017665
C	1.021546	1.605581	-0.018370
C	-0.288619	2.028310	-0.033104
C	-1.372528	1.116837	-0.009296
C	-1.153840	-0.244700	0.014701
O	0.582398	-1.968614	-0.089607
H	1.898004	-1.594612	-0.092381
N	2.360979	-0.506004	0.095364
H	1.849175	2.301878	-0.013018
H	-0.509690	3.088116	-0.037736
H	-2.392698	1.478968	0.001647
F	-2.188046	-1.101337	0.051326

MECP

B3LYP (E = -460.888293; ZPVE = 0.0840)   CASSCF(8,8) (E = -458.250949; ZPVE = 0.089486)

Triplet Occupation: **29** - 1.89; **30** - 1.95; **31 -** 1.91; **32** - 1.00;

33 - 1.00; **34** - 0.10; **35** - 0.10; **36 -** 0.04

Singlet Occupation: **29** - 1.94; **30** - 1.97; **31 -** 1.88; **32** - 1.91;

33 - 0.13; **34** - 0.03; **35** - 0.07; **36** - 0.06

C	0.097463	-0.758423	0.007280	0.114275	-0.750916	0.008232
C	1.412020	-0.053653	0.003939	1.430873	-0.062799	0.005876
C	1.395259	1.396964	0.004944	1.401490	1.401969	0.005957
C	0.208741	2.059198	0.013092	0.216953	2.060141	0.013471
C	-1.030607	1.346228	0.008278	-1.051991	1.341828	0.009987
C	-1.093131	-0.019729	0.001573	-1.107538	-0.010947	0.004802
O	0.195628	-2.041699	0.013844	0.193450	-2.003310	0.011251
H	1.257062	-2.097765	0.015605	1.236337	-2.089038	0.011595
N	2.421414	-0.842784	0.003710	2.412800	-0.873229	0.005467
H	2.346971	1.912342	0.001600	2.341534	1.919145	0.000316
H	0.172542	3.140690	0.019116	0.176318	3.132976	0.017612
H	-1.965439	1.895893	0.009212	-1.974550	1.892237	0.006859
F	-2.281917	-0.650391	0.006190	-2.253943	-0.671188	-0.005413

5. References

(S1) Pirali, T.; Gatti, S.; Di Brisco, R.; Tacchi, S.; Zaninetti, R.; Brunelli, E.; Massarotti, A.; Sorba, G.; Canonico, P. L.; Moro, L.; Genazzani, A. A.; Tron, G. C.; Billington, R. A. Estrogenic Analogues Synthesized by Click Chemistry. *ChemMedChem* **2007**, *2*, 437–440.

(S2) Vosko, S. H.; Wilk, L.; Nusair, M. Accurate Spin-Dependent Electron Liquid Correlation Energies for Local Spin Density Calculations: A Critical Analysis. *Can. J. Phys.* **1980**, *58*, 1200–1211.

(S3) Lee, C.; Yang, W.; Parr, R. G. Development of the Colle-Salvetti Correlation-Energy Formula into a Functional of the Electron Density. *Phys. Rev. B* **1988**, *37*, 785–789.

(S4) Becke, A. D. Density-Functional Thermochemistry. III. The Role of Exact Exchange. *J. Chem. Phys.* **1993**, *98*, 5648–5652.

(S5) Frisch, M. J.; Pople, J. A.; Binkley, J. S. Self-Consistent Molecular Orbital Methods 25. Supplementary Functions for Gaussian Basis Sets. *J. Chem. Phys.* **1984**, *80*, 3265–3269.

(S6) Frisch, M. J.; Trucks, G. W.; Schlegel, H. B.; Scuseria, G. E.; Robb, M. A.; Cheeseman, J. R.; Scalmani, G.; Barone, V.; Petersson, G. A.; Nakatsuji, H.; Li, X.; Caricato, M.; Marenich, A. V.; Bloino, J.; Janesko, B. G.; Gomperts, R.; Mennucci, B.; Hratchian, H. P.; Ortiz, J. V.; Izmaylov, A. F.; Sonnenberg, J. L.; Williams-Young, D.; Ding, F.; Lipparini, F.; Egidi, F.; Goings, J.; Peng, B.; Petrone, A.; Henderson, T.; Ranasinghe, D.; Zakrzewski, V. G.; Gao, J.; Rega, N.; Zheng, G.; Liang, W.; Hada, M.; Ehara, M.; Toyota, K.; Fukuda, R.; Hasegawa, J.; Ishida, M.; Nakajima, T.; Honda, Y.; Kitao, O.; Nakai, H.; Vreven, T.; Throssell, K.; Montgomery, J. A., Jr.; Peralta, J. E.; Ogliaro, F.; Bearpark, M. J.; Heyd, J. J.; Brothers, E. N.; Kudin, K. N.; Staroverov, V. N.; Keith, T. A.; Kobayashi, R.; Normand, J.; Raghavachari, K.; Rendell, A. P.; Burant, J. C.; Iyengar, S. S.; Tomasi, J.; Cossi, M.; Millam, J. M.; Klene, M.; Adamo, C.; Cammi, R.; Ochterski, J. W.; Martin, R. L.; Morokuma, K.; Farkas, O.; Foresman, J. B.; Fox, D. J. Gaussian 16, Revision B.01; Gaussian, Inc.: Wallingford CT, 2016.

(S7) Nunes, C. M.; Eckhardt, A. K.; Reva, I.; Fausto, R.; Schreiner, P. R. Competitive Nitrogen versus Carbon Tunneling. *J. Am. Chem. Soc.* **2019**, *141*, 14340–14348.

(S8) Barone, V.; Bloino, J.; Guido, C. A.; Lipparini, F. A Fully Automated Implementation of VPT2 Infrared Intensities. *Chem. Phys. Lett.* **2010**, *496*, 157–161.

(S9)   Bloino, J.; Barone, V. A Second-Order Perturbation Theory Route to Vibrational Averages and Transition Properties of Molecules: General Formulation and Application to Infrared and Vibrational Circular Dichroism Spectroscopies. *J. Chem. Phys.* **2012**, *136*, 124108.

(S10)   Barone, V.; Biczysko, M.; Bloino, J. Fully Anharmonic IR and Raman Spectra of Medium-Size Molecular Systems: Accuracy and Interpretation. *Phys. Chem. Chem. Phys.* **2014**, *16*, 1759–1787.

(S11)   Montgomery, J. A.; Frisch, M. J.; Ochterski, J. W.; Petersson, G. A. A Complete Basis Set Model Chemistry. VI. Use of Density Functional Geometries and Frequencies. *J. Chem. Phys.* **1999**, *110*, 2822–2827.

(S12)   Montgomery, J. A.; Frisch, M. J.; Ochterski, J. W.; Petersson, G. A. A Complete Basis Set Model Chemistry. VII. Use of the Minimum Population Localization Method. *J. Chem. Phys.* **2000**, *112*, 6532–6542.

(S13)   Schachtschneider, J. H.; Mortimer, F. S. Vibrational Analysis of Polyatomic Molecules. VI. FORTRAN IV Programs for Solving the Vibrational Secular Equation and for the Least-Squares Refinement of Force Constants, Structural Interpretation Of Spectra. Shell Development Co., Emeryville, CA, 1969.

(S14)   Pulay, P.; Fogarasi, G.; Pang, F.; Boggs, J. E. Systematic AB Initio Gradient Calculation of Molecular Geometries, Force Constants, and Dipole Moment Derivatives. *J. Am. Chem. Soc.* **1979**, *101*, 2550–2560.

(S15)   Karney, W. L.; Borden, W. T. Ab Initio Study of the Ring Expansion of Phenylnitrene and Comparison with the Ring Expansion of Phenylcarbene. *J. Am. Chem. Soc.* **1997**, *119*, 1378–1387.

(S16)   Smith, K. M.; Poli, R.; Harvey, J. N. Ligand Dissociation Accelerated by Spin State Change: Locating the Minimum Energy Crossing Point for Phosphine Exchange in $CpMoCl_2(PR_3)_2$ Complexes. *New J. Chem.* **2000**, *24*, 77–80.

(S17)   Harvey, J. N. Understanding the Kinetics of Spin-Forbidden Chemical Reactions. *Phys. Chem. Chem. Phys.* **2007**, *9*, 331–343.

(S18)   Rodríguez-Guerra, J.; Funes-Ardoiz, I.; Maseras, F. EasyMECP. Zenodo 2018.

(S19)   Harvey, J. N.; Aschi, M.; Schwarz, H.; Koch, W. The Singlet and Triplet States of Phenyl Cation. A Hybrid Approach for Locating Minimum Energy Crossing Points between Non-Interacting Potential Energy Surfaces. *Theor. Chem. Acc.* **1998**, *99*, 95–99.

(S20) Gannon, K. L.; Blitz, M. A.; Liang, C. H.; Pilling, M. J.; Seakins, P. W.; Glowacki, D. R.; Harvey, J. N. An Experimental and Theoretical Investigation of the Competition between Chemical Reaction and Relaxation for the Reactions of $^1CH_2$ with Acetylene and Ethene: Implications for the Chemistry of the Giant Planets. *Faraday Discuss.* **2010**, *147*, 173–188.

(S21) Viegas, L. P.; M. Nunes, C.; Fausto, R. Spin-Forbidden Heavy-Atom Tunneling in the Ring-Closure of Triplet Cyclopentane-1,3-Diyl. *Phys. Chem. Chem. Phys.* **2021**, *23*, 5797–5803.

(S22) Vyas, S.; Winter, A. H.; Hadad, C. M. Chapter 2. Theory and Computation in the Study of Nitrenes and Their Excited-State Photoprecursors. In *Nitrenes and Nitrenium ions*; Falvey, D. E., Gudmundsdottir, A. D., Eds.; Wiley, **2013**; pp 33–76.

(S23) Wentzel, G. Eine Verallgemeinerung Der Quantenbedingungen Für Die Zwecke Der Wellenmechanik. *Zeitschrift für Phys.* **1926**, *38*, 518–529.

(S24) Kramers, H. A. Wellenmechanik Und Halbzahlige Quantisierung. *Zeitschrift für Phys.* **1926**, *39*, 828–840.

(S25) Brilluoin, L. La Mécanique Ondulatoire de Schrödinger; Une Méthode Générale de Résolution Par Approximations Successives. *C. R. Acad. Sci* **1926**, *183*, 24–26.

(S26) Delos, J. B. On the Reactions of N_2 with O. *J. Chem. Phys.* **1973**, *59*, 2365–2369.

(S27) Landau, L. D.; Lifshitz, E. M. *Quantum Mechanics. Non-Relativistic Theory*; (Pergamon Press Ltd., Oxford, England), Second (Revised) Edition, **1965**.

(S28) Coveney, P. V.; Child, M. S.; Bárány, A. The Two-State S Matrix for the Landau-Zener Potential Curve Crossing Model: Predissociation and Resonant Scattering. *J. Phys. B At. Mol. Phys.* **1985**, *18*, 4557–4580.

(S29) Harvey, J. N.; Aschi, M. Spin-Forbidden Dehydrogenation of Methoxy Cation: A Statistical View. *Phys. Chem. Chem. Phys.* **1999**, *1*, 5555–5563.

(S30) Tully, J. C. Collision Complex Model for Spin Forbidden Reactions: Quenching of $O(^1D)$ by N_2. *J. Chem. Phys.* **1974**, *61*, 61–68.

(S31) Zahr, G. E.; Preston, R. K.; Miller, W. H. Theoretical Treatment of Quenching in $O(^1D)$ + N_2 Collisions. *J. Chem. Phys.* **1975**, *62*, 1127–1135.

(S32) Heller, E. J.; Brown, R. C. Radiationless Transitions in a New Light. *J. Chem. Phys.* **1983**, *79*, 3336–3351.

(S33) Lorquet, J. C.; Leyh-Nihant, B. Nonadiabatic Unimolecular Reactions. 1. A Statistical Formulation for the Rate Constants. *J. Phys. Chem.* **1988**, *92*, 4778–4783.

(S34) Cui, Q.; Morokuma, K.; Bowman, J. M.; Klippenstein, S. J. The Spin-Forbidden Reaction Nonadiabatic Transition State Theory and Application. *J. Chem. Phys.* **1999**, *110*, 9469–9482.

(S35) Nunes, C. M.; Viegas, L. P.; Wood, S. A.; Roque, J. P. L.; McMahon, R. J.; Fausto, R. Heavy-Atom Tunneling Through Crossing Potential Energy Surfaces: Cyclization of a Triplet 2-Formylarylnitrene to a Singlet 2,1-Benzisoxazole. *Angew. Chem. Int. Ed.* **2020**, *59*, 17622–17627.

(S36) Chiodo, S.; Russo, N. Determination of Spin-Orbit Coupling Contibutions in the Framework of Density Functional Theory. *J. Comput. Chem.* **2008**, *29*, 912–920.

(S37) Chiodo, S. G.; Russo, N. One Electron Spin Orbit Contribution by Effective Nuclear Charges. *J. Comput. Chem.* **2009**, *30*, 832–839.

(S38) Chiodo, S. G.; Leopoldini, M. MolSOC: A Spin-Orbit Coupling Code. *Comput. Phys. Commun.* **2014**, *185*, 676–683.